VOLUME 32 | SUPPLEMENT 2 | MARCH 2019

MODERN PATHOLOGY

USCAP 2019

ABSTRACTS

NEUROPATHOLOGY AND OPHTHALMIC PATHOLOGY (1621-1666)

USCAP 108TH ANNUAL MEETING

UNLOCKING YOUR INGENUITY

MARCH 16-21, 2019

National Harbor, Maryland
Gaylord National Resort & Convention Center

Published by
SPRINGER NATURE
www.ModernPathology.org

USCAP Creating a Better Pathologist
AN OFFICIAL JOURNAL OF THE UNITED STATES AND CANADIAN ACADEMY OF PATHOLOGY

EDUCATION COMMITTEE

Jason L. Hornick, Chair
Rhonda K. Yantiss, Chair, Abstract Review Board and Assignment Committee
Laura W. Lamps, Chair, CME Subcommittee
Steven D. Billings, Interactive Microscopy Subcommittee
Shree G. Sharma, Informatics Subcommittee
Raja R. Seethala, Short Course Coordinator
Ilan Weinreb, Subcommittee for Unique Live Course Offerings
David B. Kaminsky (Ex-Officio)
Aleodor (Doru) Andea
Zubair Baloch
Olca Basturk
Gregory R. Bean, Pathologist-in-Training
Daniel J. Brat
Ashley M. Cimino-Mathews
James R. Cook
Sarah M. Dry
William C. Faquin
Carol F. Farver
Yuri Fedoriw
Meera R. Hameed
Michelle S. Hirsch
Lakshmi Priya Kunju
Anna Marie Mulligan
Rish Pai
Vinita Parkash
Anil Parwani
Deepa Patil
Kwun Wah Wen, Pathologist-in-Training

ABSTRACT REVIEW BOARD

Benjamin Adam
Michelle Afkhami
Narasimhan (Narsi) Agaram
Rouba Ali-Fehmi
Ghassan Allo
Isabel Alvarado-Cabrero
Christina Arnold
Rohit Bhargava
Justin Bishop
Jennifer Boland
Elena Brachtel
Marilyn Bui
Shelley Caltharp
Joanna Chan
Jennifer Chapman
Hui Chen
Yingbei Chen
Benjamin Chen
Rebecca Chernock
Beth Clark
James Conner
Alejandro Contreras
Claudiu Cotta
Timothy D'Alfonso
Farbod Darvishian
Jessica Davis
Heather Dawson
Elizabeth Demicco
Suzanne Dintzis
Michelle Downes
Daniel Dye
Andrew Evans
Michael Feely
Dennis Firchau
Larissa Furtado
Anthony Gill
Ryan Gill
Paula Ginter
Tamara Giorgadze
Raul Gonzalez
Purva Gopal
Anuradha Gopalan
Jennifer Gordetsky
Rondell Graham
Alejandro Gru
Nilesh Gupta
Mamta Gupta
Krisztina Hanley
Douglas Hartman
Yael Heher
Walter Henricks
John Higgins
Mai Hoang
Mojgan Hosseini
Aaron Huber
Peter Illei
Doina Ivan
Wei Jiang
Vickie Jo
Kirk Jones
Neerja Kambham
Chiah Sui (Sunny) Kao
Dipti Karamchandani
Darcy Kerr
Ashraf Khan
Rebecca King
Michael Kluk
Kristine Konopka
Gregor Krings
Asangi Kumarapeli
Alvaro Laga
Cheng-Han Lee
Zaibo Li
Haiyan Liu
Xiuli Liu
Yan-Chun Liu
Tamara Lotan
Anthony Magliocco
Kruti Maniar
Jonathan Marotti
Emily Mason
Jerri McLemore
Bruce McManus
David Meredith
Anne Mills
Neda Moatamed
Sara Monaco
Atis Muehlenbachs
Bita Naini
Dianna Ng
Tony Ng
Ericka Olgaard
Jacqueline Parai
Yan Peng
David Pisapia
Alexandros Polydorides
Sonam Prakash
Manju Prasad
Peter Pytel
Joseph Rabban
Stanley Radio
Emad Rakha
Preetha Ramalingam
Priya Rao
Robyn Reed
Michelle Reid
Natasha Rekhtman
Michael Rivera
Michael Roh
Andres Roma
Avi Rosenberg
Esther (Diana) Rossi
Peter Sadow
Safia Salaria
Steven Salvatore
Souzan Sanati
Sandro Santagata
Anjali Saqi
Frank Schneider
Jeanne Shen
Jiaqi Shi
Wun-Ju Shieh
Gabriel Sica
Deepika Sirohi
Kalliopi Siziopikou
Lauren Smith
Sara Szabo
Julie Teruya-Feldstein
Gaetano Thiene
Khin Thway
Rashmi Tondon
Jose Torrealba
Evi Vakiani
Christopher VandenBussche
Sonal Varma
Endi Wang
Christopher Weber
Olga Weinberg
Sara Wobker
Mina Xu
Shaofeng Yan
Anjana Yeldandi
Akihiko Yoshida
Gloria Young
Minghao Zhong
Yaolin Zhou
Hongfa Zhu
Debra Zynger

1621 Expression of Notch Signaling in Lacrimal Gland Adenoid Cystic Carcinoma

Shahzan Anjum[1], Seema Sen[2], Kunzang Chosdol[1], Sameer Bakhshi[1], Seema Kashyap[1], Neelam Pushker[1], Mandeep Bajaj[1], Mehar Sharma[1], Rachna Meel[1]
[1]All India Institute of Medical Sciences, New Delhi, India, [2]New Delhi, India

Disclosures: Shahzan Anjum: None; Rachna Meel: None

Background: Adenoid Cystic Carcinoma (ACC) is the commonest epithelial malignant tumour of lacrimal gland associated with high risk of local recurrence & distance metastasis. There is no specific treatment for this tumor due to lack of well characterized molecular markers. Although Notch signaling is well established in salivary gland ACC, role of Notch signaling in lacrimal gland ACC has not been explored. The present study aims to evaluate the status of Notch1 in ACC & to correlate it with clinicopathological high risk features.

Design: Nine prospective cases of histopathologocally proven lacrimal gland ACC & 5 normal lacrimal gland samples were included in this study. Tumor staging was done by AJCC,2007. Histologic classification was divided into cribriform, tubular & solid patterns. 18 months follow up was available. Protein expression of Notch1 was evaluated by immunohistochemistry (IHC) using monoclonal antibody (clone: D1E11). Gene expression analysis of Notch1gene was done by quantitative real time PCR. The relative mRNA expression of Notch1 in tumour samples with respect to normal lacrimal gland was calculated by ΔΔCt method.

The results were correlated with clinicopathological high risk features and follow-up.

Results: Of the nine cases of lacrimal gland ACC, there were 8 females & one male with a mean age of 38 years (±25.8). Right eye was involved in 67% (6/9) patients. The main histologic growth pattern was cribriform (n=5) while solid pattern was observed in one case. Perineural invasion was found in 3 (33%) cases. Recurrence occurred in 33% cases (3/9), lymph node & systemic metastasis in 2/9 cases (22%) & two patients with metastasis died. Advance T stage (>T2) was found in 67% cases (6/9). Cytoplasmic overexpression of Notch1 was detected in 88% (8/9) cases. No statistically significant correlation was found between protein expression of Notch1 &clinicopathological high risk features. Gene expression analysis of all 9 cases showed upregulation in 78% cases (7/9). Kaplan Meier survival analysis showed significant association of poor disease free survival with perineural invasion (p = 0.045) & advance T stage (p= 0.045).

Conclusions: Overexpression of Notch1 protein & gene was observed in 88% & 78% ACC cases respectively in this study. A poor disease free survival was found to be significantly associated with perineural invasion (p=0.045) & advance T stage (p=0.045). A larger patient cohort would give better insight into role of Notch 1 as a prognostic & therapeutic target.

1622 Characterization of Infiltrating Gliomas by the Oncoscan CNV Plus Assay and Comparison to Next-Generation Sequencing (NGS) and Fluorescent in Situ Hybridization (FISH) data

Christina Appin[1], Qinwen Mao[2], Eileen Bigio[3], Daniel Brat[3], Craig Horbinski[4], Xinyan Lu[4]
[1]Northwestern University, Chicago, IL, [2]Northwestern Medicine, Chicago, IL, [3]Northwestern University Feinberg School of Medicine, Chicago, IL, [4]Chicago, IL

Disclosures: Christina Appin: None; Qinwen Mao: None; Eileen Bigio: None; Daniel Brat: None; Craig Horbinski: None; Xinyan Lu: None

Background: Infiltrating gliomas include astrocytomas (WHO grades II-IV) and oligodendrogliomas (WHO grades II-III). These tumors are incurable by surgical resection and eventually progress to higher grade tumors. In recent years, molecular and cytogenetic profiling including fluorescent in situ hybridization (FISH), next-generation sequencing (NGS), and SNP microarrays have enabled the genomic characterization of these tumors for further classification.

Design: We integrated FISH, NGS and the SNP Oncoscan assay to assess the genomic aberrations in brain tumors for molecular classification. We correlated the Oncoscan data with the NGS and FISH data.

Results: We included 35 infiltrating gliomas in the study. There were 20 glioblastomas (GBMs), 5 anaplastic astrocytomas, 1 diffuse astrocytoma, and 9 oligodendrogliomas, 5 of which were anaplastic cases. All 35 cases were assessed for copy number aberrations (CNAs) using OncoScan. NGS and FISH for 1p/19q co-deletion were performed on 32 and 10 of the tumors, respectively. Of the infiltrating astrocytomas, 20 were IDH-wildtype and 6 were IDH-mutant. The Oncoscan CNV Plus Assay detected 83 of the 86 copy number variations that were detected by NGS, showing a 96.5% correlation. All cases of 1p/19q co-deletion detected by FISH (8 cases) were detected by the Oncoscan assay and the two cases that were negative by FISH (2 cases) were also negative by Oncoscan, showing 100% concordance. IDH-wildtype GBMs and anaplastic astrocytomas showed the most complex cytogenetic profiles, with the most frequent alterations being partial deletions, seen in 100% of the tumors, followed by whole chromosome deletions (85%), partial gains (80%), whole chromosome gains (70%), and amplification events (65%). Copy neutral loss of heterozygosity (LOH) was less common (30%). All IDH-mutant astrocytomas showed less frequent partial deletions, copy neutral LOH, and partial gains however, whole chromosome deletions were seen in 67%. Oligodendrogliomas were characterized by whole chromosome arm losses of 1p and 19q, with very few isolated partial gains

and deletions and no amplification events. Anaplastic oligodendrogliomas showed whole chromosome deletions and copy neutral LOH events that were not seen in grade 2 tumors.

Conclusions: Although the sample size for the study is limited, our data showed great correlation between the Oncoscan CNV Plus Assay and NGS or FISH. The integrated molecular profiling provides comprehensive evaluation and classification of infiltrating gliomas.

1623 Dedifferentiated Chordoma of the Clivus: A Monocentric Experience

Sofia Asioli[1], Alberto Righi[2], Francesca Ambrosi[3], Costantino Ricci[4], Matteo Zoli[5], Ernesto Pasquini[6], Diego Mazzatenta[1], Maria Foschini[1]
[1]University of Bologna, Bologna, Italy, [2]Rizzoli Institute, Bologna, Italy, [3]S.Orsola-Malpighi Hospital, University of Bologna, Bari, Italy, [4]S.Orsola-Malpighi Hospital, University of Bologna, Bologna, Italy, [5]IRCCS Istituto delle Scienze Neurologiche di Bologna, Bologna, Italy, [6]University of Bologna, Castel Maggiore, Italy

Disclosures: Sofia Asioli: None; Alberto Righi: None; Francesca Ambrosi: None; Costantino Ricci: None; Matteo Zoli: None; Ernesto Pasquini: None; Diego Mazzatenta: None; Maria Foschini: None

Background: Dedifferentiated chordoma (DC) is a biphasic malignant tumor, that occurs almost exclusively in recurrent disease or after radiotherapy treatment, with a strong predilection for sacrum area. DC localized in the clivus are extremely rare and limited to a case report.

Design: We investigated the morphological, immunohistochemical features of 6 DCs of the clivus and their clinical behavior in patients treated in a single institution between 1998 and 2017.

Results: These 6 cases (4 males, 2 females) represent 8.1% of series of 74 clivus chordoma surgically treated in our institution. Age ranged from 35 to 64 years (mean: 46 years). Three out of these 6 patients have been previously undergone surgery followed to radiotherapy with a histological diagnosis of chordoma without areas of dedifferentiation, whereas in two other cases a biopsy was done in other centers with a diagnosis of classic chordoma. Five patients had diplopia, one patient had dysphasia and hemiparesis and the remaining case had dysphagia. DCs were extradural in 5 cases, and only one presented an intradural extension. All cases were operated through an endoscopic endonasal approach with a subtotal tumor removal in 3 cases, and a partial tumor removal in 3 cases. Morphologically, all cases showed two distinct components: a classic chordoma juxtaposed to dedifferentiated component without notochordal differentiation constituted to high grade undifferentiated spindle or pleomorphic sarcoma. Immunohistochemically, the tumor cells of classic chordomas component were positive for brachyury, S-100 protein, and epithelial markers including pan-cytokeratins and EMA; whereas dedifferentiated tumor cells were negative for all markers examined, including also muscle markers (smooth muscle actin, desmin, h-caldesmon and myogenin) and osteogenic marker SATB2. INI1 protein nuclear expression, that is usually lost in poorly differentiated chordoma, was maintained in both components of all 6 cases. All patients were treated with proton beam therapy or other radiotherapies after surgery. One patient presented a consistent progression of the remnant after 12 months, which requires a second surgery through the same approach. All patients died of disease with tumor progression after a mean of 29 months (range from 11to 52 months).

Conclusions: DC is not so rare aggressive neoplasm in the clivus, resistant to conventional radiation treatment. It usually developed from recurrence or progression of a classic chordoma after surgical approach or radiation therapy, although de novo cases exist

1624 High caveolin-1 expression is associated with increased risk of recurrence in meningiomas

Javier Baena-Del Valle[1], Anderson J. Remolina[2], Enrique C Ramos-Clason[3], Ariaris Avello-Malaver[4], Doris E. Gomez-Camargo[3], Martha C Tuñon-Pitalua[3]
[1]Fundacion Santa Fe de Bogota, Bogota, Colombia, [2]University of Cartagena, Bucaramanga, Bolivar, Colombia, [3]University of Cartagena, Cartagena, Bolivar, Colombia, [4]Fundacion Santa Fe de Bogota, Bogotá, Colombia

Disclosures: Javier Baena-Del Valle: None; Anderson J. Remolina: None; Enrique C Ramos-Clason: None; Ariaris Avello-Malaver: None; Doris E. Gomez-Camargo: None; Martha C Tuñon-Pitalua: None

Background: Caveolin-1 (CAV1) is an integral membrane protein that constitutes the main structural component of caveolae, specialized microdomains involved in many cell signaling and transport processes. The role of CAV1 in tumorigenesis is controversial, in some cancers (e.g. kidney, prostate, head and neck) high expression has been associated with worse prognosis, while in others (e.g. lung and esophageal adenocarcinomas) it has tumor suppressor activity. Although there is growing evidence of the role of CAV1 in brain tumors, very few studies have focused on meningiomas. These neoplasms account for more than 30% of intracranial tumors. While most patients will be cured after tumor excision, a minority will recur regardless of histologic grade, size and localization. There is general lack of knowledge about factors involved in meningiomas recurrence, therefore research on prognostic markers is necessary. The aim of this study was to determine CAV1 expression in meningiomas and to perform a clinic-pathological correlation.

Design: Anatomopathological samples and clinical records obtained from 128 patients attending to the Fundación Centro Colombiano de Epilepsia y Enfermedades Neurológicas – FIRE (Cartagena, Colombia) in a 10-year period were included in this cross sectional study. Slides were reviewed by expert pathologists and tissue microarrays were constructed. CAV1 expression was determined by immunohistochemistry using caveolin-1 Antibody (N-20): sc-894 (1:500) (Santa Cruz Biotechnology) and analyzed by quantitative image analysis (color deconvolution - ImageJ).

Results: WHO grade II meningiomas showed higher CAV1 expression than WHO grade I tumors (p = 0.049). Median CAV1 expression was higher in recurrent tumors (0.0250) than in non-recurrent ones (0.0188) (p = 0.0435). Receiver Operating Characteristic (ROC) curve analysis to evaluate the role of CAV1 as a predictor of recurrence in meningiomas showed a cut-off point >0.022, with a sensitivity and specificity of 63.2% and 64.7%, respectively. Area under the curve (AUC) = 0.640 (confidence interval 95% = 0.518 – 0.750), p= 0.0311.

Figure 1 - 1624

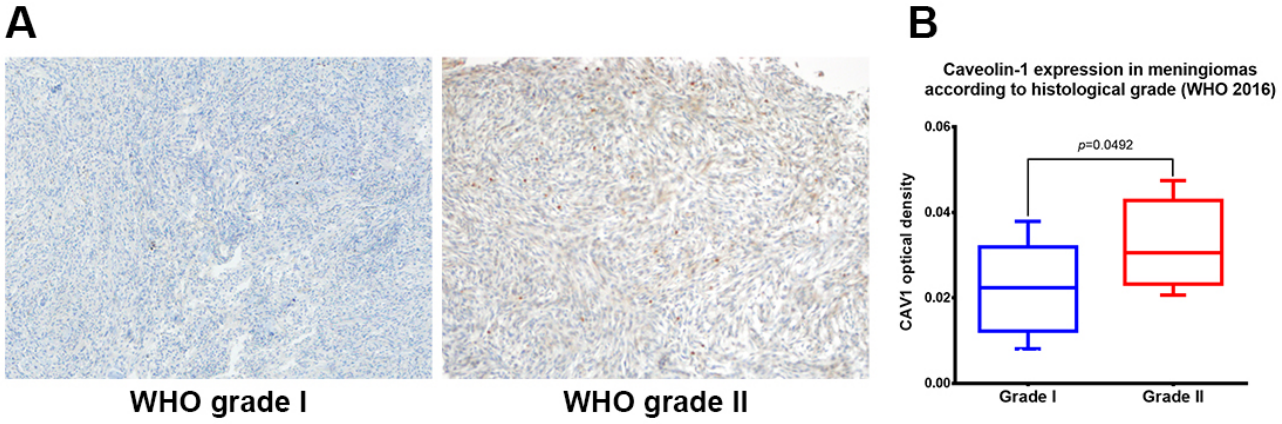

Conclusions: These findings show that high expression of CAV1 is frequent in atypical meningiomas and it is associated with increased risk of recurrence. Our results contribute to the hypothesis that high CAV1 expression may be an indicator of biologic aggressiveness in meningiomas, becoming a potentially useful biomarker in clinical practice.

1625 Molecular Characterization of Sporadic Cerebral Cavernous Malformations

Jordan Baum[1], Hung Tran[2], Wei Song[3], David Pisapia[4]
[1]Weill Cornell Medicine, New York, NY, [2]Weill Cornell Medicine, Flushing, NY, [3]Weill Cornell Medical College, Short Hills, NJ, [4]New York, NY

Disclosures: Jordan Baum: None; Hung Tran: None; Wei Song: None; David Pisapia: None

Background: Cerebral cavernous malformations (CCavMal) are benign vascular proliferations that may present sporadically or as part of a familial syndrome with an autosomal dominant inheritance pattern. Loss-of-function mutations in three genes, *KRIT1* (*CCM1*), *CCM2*, and *PDCD10* (*CCM3*), cause the majority of familial cerebral cavernous malformations. Given that studies of non-cerebral venous malformations found recurrent hotspot mutations in the oncogenes *TEK* and *PIK3CA*, we hypothesized that similar alterations may be present in sporadic CCavMal.

Design: 12 cases of sporadic CCavMal with sufficient DNA were selected from the specimen archives from 1/2014 to 1/2018. None of the patients had a family history of CCavMal. Unstained slides from formalin-fixed paraffin embedded blocks were macrodissected. 11 cases underwent next-generation sequencing (NGS) using the Oncomine Comprehensive assay (v2) and in one case NGS was performed using the Ion Torrent Ampliseq Cancer Hotspot Panel (v2). PCR amplification and Sanger sequencing of exon 17 of *TEK* were performed on all cases.

Results: Hotspot gain-of-function *PIK3CA* mutations in codons 542 (2 cases), 545 (1 case), 1047 (1 case), and 1049 (1 case) were identified for a total of 5 out of 12 cases (42%). In one case lacking *PIK3CA* mutation, amplification of *FGFR* was identified, and in one case with a *PIK3CA* mutation a *PTPN11* p.Ala72Val mutation was identified at a similar variant allele frequency to that of the *PIK3CA* alteration. No exon 17 *TEK* mutations were detected in this cohort. Interestingly, two cases without identified alterations occurred in patients with multiple CCavMal, and the possibility of mutations in *KRIT1*, *CCM2*, or *PDCD10* should be explored.

Conclusions: Recurrent alterations of *PIK3CA* were identified in a high percentage of sporadic CCavMal in this small cohort (5/12 cases). A single case demonstrated amplification of *FGFR* while *TEK* mutations were not identified in this cohort. These findings may prove to be of diagnostic utility in distinguishing sporadic from inherited cases, or when the histological findings of CCavMal are ambiguous. Moreover,

given that vascular malformations have been successfully treated in mouse models using pharmacological inhibitors of the PIK3CA pathway and that clinical trials are underway in FGFR-driven solid tumors, these findings may hold important treatment implications for patients with CCavIMal, especially in patients who are not surgical candidates.

1626 Incidence of Corneal Diseases in a Large Ocular Pathology Centre: A 10 Year Review

Sabrina Bergeron[1], Miguel Burnier[2], Julia Burnier[3]
[1]The MUHC - McGill University Ocular Pathology Laboratory & Translational Research Laboratory, Montreal, QC, [2]MUHC - McGill University Ocular Pathology Laboratory, Montreal, QC, [3]The MUHC - McGill University Ocular Pathology & Translational Research Laboratory, Montreal, QC

Disclosures: Sabrina Bergeron: None; Miguel Burnier: None

Background: In ocular pathology, corneal specimens account for about 13% of all pathological samples, representing a significant portion of the workload. As the cornea is generally not affected by neoplastic disease, its histopathology may be overlooked in practices not specialized in ocular pathology.

This study aims to highlight the prevalence and incidence of corneal diseases in ocular pathology with emphasis on diagnoses that are unique to cornea such as keratoconus, ICE syndrome, Salzmann nodule, stromal dystrophy and corneal intraepithelial neoplasia (CIN).

Design: A single-centre, retrospective analysis of 865 corneal specimens received between 2006-2017 was performed. Specimens were sorted by diagnosis (Table I), and grouped by age and sex.

Results: Inflammatory disease represent 44% of cases (n=380), with comparable incidence for men and women (n=198 and n=182, respectively). Dystrophies and degenerations represent 30% of cases (n=267) with a slight predominance in men (n=152) when compared to women (n=115). Corneas from failed graft make up 16% of cases (n=141) with equal representation of sexes. Infection by viruses or microorganisms represent 6% of total cases (n=51) and 71% were from male patients. HSV infection represents 80% of all infectious cases. Neoplastic changes in the cornea typically arise from extension of conjunctival neoplasia across the limbal area (n=19) or from CIN (n=7) and represent 3% of cases with comparable distribution between men and women.

PAS stain highlights the basement membrane of the epithelium, the Descemet and the presence of polysaccharide in the stroma; a PAS stain is recommended for routine examination of all corneal dystrophies.

Histopathological findings for HSV keratitis were chronic inflammation with vascularization of the stroma. Subepithelial pannus, bullae and ulceration is often present. IHC against HSV I/II was performed on 14/40 cases; only 35% of them stained positive. IHC for HSV is only reliable for cases showing acute exacerbation; diagnosis of HSV keratitis relies mainly on clinico-pathological correlation.

	# cases	% total
Inflam	**380**	**43.9%**
Keratitis/Fibrosis/Oedema	308	35.6%
Ulceration/perforation/scar	72	8.3%
Dystrophy/degeneration	**267**	**30.9%**
Keratoconus	99	11.4%
Bullous	59	6.8%
Fuch's	48	5.5%
Stromal dystrophy	27	3.1%
Salzmann nodule	10	1.2%
ICE syndrome	8	0.9%
Band keratopathy	6	0.7%
Epithelial dystrophy	4	0.5%
Amyloid	2	0.2%
Cystinosis	2	0.2%
Pemphigoid	2	0.2%
Failed graft	**141**	**16.3%**
Microorganisms	**51**	**5.9%**
HSV	40	4.6%
Bacterial undefined	4	0.5%
Acanthamoeba	3	0.3%
Actinomyces	1	0.1%
Syphilis	1	0.1%
Gonhorrea	1	0.1%
Aspergillus	1	0.1%
Benign	**26**	**3.0%**
Acanthosis	12	1.4%
CIN	7	0.8%
Pterygium/pinguecula	3	0.3%
Conjunctivalisation	2	0.2%
Papilloma	1	0.1%
Inclusion cyst	1	0.1%
Grand Total	**865**	**100.0%**

Conclusions: Inflammatory disease, whether infectious or not, represents the majority of consultations for corneal disease, followed by corneal dystrophies and degenerations. Due to the avascular nature of the cornea, neoplasia is very rare.

In cases suspicious of dystrophies, a PAS stain is routinely recommended. The use of IHC against HSV is not deemed necessary as it only indicates an acute phase of the infection.

1627 GATA3 as a New Marker of Gonadotroph Adenomas

Samuel Bidot[1], Abigail Goodman[2], Lindsey Lowder[3], Jose Velazquez Vega[4], Stephen Hunter[2], Stewart Neill[5], Matthew Schniederjan[6]
[1]Emory University School of Medicine, Atlanta, GA, [2]Emory University Hospital, Atlanta, GA, [3]Emory University School of Medicine, Tucker, GA, [4]Children's Healthcare of Atlanta, Atlanta, GA, [5]Emory University Medicine, Decatur, GA,[6]Dunwoody, GA

Disclosures: Samuel Bidot: None; Abigail Goodman: None; Lindsey Lowder: None; Jose Velazquez Vega: None; Stephen Hunter: None; Stewart Neill: None; Matthew Schniederjan: None

Background: Pituitary adenomas are among the most common surgical neuropathology specimens and constitute the majority of sellar region masses. Subtyping adenomas by immunohistochemical (IHC) hormone expression informs clinical management and expectations, yet is complicated by low or absent staining in some adenomas, particularly gonadotrophs. Steroidogenic factor-1 (SF1) is a transcription factor sometimes used to identify gonadotroph adenomas, but is a technically challenging immunostain and not widely available. GATA proteins, particularly GATA-2, are known to regulate gene expression and have been hypothesized to contribute to gonadotroph differentiation, and could serve as markers of gonadotroph phenotype. Here we analyze the expression of GATA3, a widely-used IHC stain for breast and urothelial carcinomas, in gonadotroph adenomas as a potential diagnostic marker for gonadotroph adenomas and readily-available surrogate for SF1 expression.

Design: Pituitary adenomas submitted for pathological examination between June and August 2018 were included in this study. IHC stains for GATA3, SF1, Pit1, Tpit (Tbx19), LH, FSH, prolactin, GH, ACTH, TSH and MIB1 (Ki-67) were performed on all cases. Adenomas were subtyped based on IHC findings in correlation with clinical history. The IHC was scored using the Allred system, and positivity was defined as a score >2. Demographic data and tumor size (determined via radiographic imaging) were retrospectively collected.

Results: A total of twenty one cases were included in this study. The mean patient age was 52 years (range: 27-80 years) and 66% of patients were female. The mean tumor size was 2.2 $\pm$ 0.9cm. The adenoma subtypes were as follows: 10 gonadotrophs (48%), 6 corticotrophs (28%), 3 somatotrophs (14%), 1 lactotroph (5%), and 1 plurihormonal adenoma (5%, PRL and TSH). GATA3 was positive in all 10 (100%) gonadotroph adenomas and 2 (18%) non-gonadotroph adenomas. The sensitivity and specificity of GATA3 in the diagnosis of gonadotroph adenoma are 100% (CI95%:69-100) and 82% (CI95%:48-98) respectively. The positive and negative predictive values are 83% (CI95%:52-98) and 100% (CI95%: 66-100); and positive and negative likelihood ratios are 5.50 (CI95%: 1.57-19.27), and 0.00, respectively.

Conclusions: GATA3 is a promising immunohistochemical marker to distinguish gonadotroph adenomas. Because GATA3 is already available in many laboratories, its utilization could help better identify gonadotroph adenomas without the need of bringing on an SF1 immunostain.

1628 Desmoplastic Infantile Ganglioglioma: A MAPK Pathway-Driven and Microglia/Macrophage-Rich Neuroepithelial Tumor

Melissa Blessing[1], Patrick Blackburn[2], Jessica Balcom[2], Chandra Krishnan[3], Virginia Harrod[4], Emily Barr Fritcher[5], Christopher Zysk[2], Rory Jackson[2], Asha Nair[2], Robert Jenkins[2], Kevin Halling[5], Benjamin Kipp[2], Amulya Nageswara Rao[2], Nadia Laack[2], Cristiane Ida[5]
[1]Mayo Clinic, Houston, TX, [2]Mayo Clinic, Rochester, MN, [3]Dell Children's Medical Center, Austin, TX, [4]Dell Children's Medical Center, Austin, TX, [5]Rochester, MN

Disclosures: Melissa Blessing: None; Patrick Blackburn: None; Jessica Balcom: None; Chandra Krishnan: None; Virginia Harrod: None; Emily Barr Fritcher: None; Christopher Zysk: None; Rory Jackson: None; Asha Nair: None; Robert Jenkins: None; Kevin Halling: None; Benjamin Kipp: None; Amulya Nageswara Rao: None; Nadia Laack: None; Cristiane Ida: None

Background: MAPK pathway activation has been recurrently reported in desmoplastic infantile ganglioglioma (DIG). The observed MAPK mutation allelic frequencies seem disproportionally low relative to the apparent typically high tumor cell content, suggesting that activating MAPK pathway alterations may be subclonal rather than driver events. We sought to expand the molecular profile of this rare tumor type and to investigate if tumor cell composition could account for the observed low mutation allelic frequencies.

Design: Comprehensive tumor molecular characterization included in-house neurooncology next generation sequencing panel, RNA sequencing, and OncoScan array. Immunohistochemical studies (CD68-PGM1, CD163, CD14, CD11c, CD3, CD20 and CD34) were performed using clinically validated protocols.

Results: Seven cases, including 4 female and 3 male, with median age at diagnosis of 3 months (range, 2-6) were evaluated. Most patients presented with enlarging head circumference. All tumors were supratentorial and post-contrast enhancing. Median estimated tumor content was 80% (range, 70-90). Activating MAPK pathway alterations were identified in 4 of 7 (57%) cases. Three tumors had a *BRAF* activating mutation (V600E, V600D and V600_W604delinsDQTDG), at 8-27% allelic frequency. A single *BRAF* wild-type tumor showed a TPM3-NRTK1 fusion associated with duplications disrupting both genes. Other copy number changes included 7p22.3p14.1 gain, 13q13.3q34 loss (with TPM3-NRTK1 fusion) and chromosome 9 loss (with *BRAF* V600E). All tumors were composed of at least 30% of cells morphologically and immunophenotypically (immunoreactive for CD68-PGM1, CD163, CD14 and CD11c) consistent with microglial/macrophage lineage. CD3 and CD20 highlighted few scattered T and rare B lymphocytes. CD34 was limited to a rich delicate vascular network. Resection was gross total and subtotal in 4 and 3 cases, respectively. Only 2 tumors (both subtotally resected) regrew and were re-excised; one of them received adjuvant treatment (chemotherapy and BRAF/MEK inhibitors), with clinical response to the targeted therapy only. Even with residual tumor, all patients are alive (median follow-up: 70 months; range 15 – 139).

Conclusions: Our study further supports DIG as another MAPK pathway-driven neuroepithelial tumor, expanding treatment options for patients with tumors not amenable to surgical cure, and suggests that DIG is a microglia/macrophage-rich neuroepithelial tumor with frequent low driver mutation allelic frequencies.

1629 Immunohistochemical analysis of PD-L1 and CD8 in brain metastases and their paired primaries: prognostic role, clinical and pathologic correlations

Florian Camy[1], Mousa Mobarki[2], Michel Peoc'H[3], Georgia Karpathiou[4]
[1]University Hospital, Saint Etienne, France, [2]North Hospital, University Hospital, Saint Etienne, France, [3]Saint Etienne, France, [4]University Hospital of Saint-Etienne, Saint-Etienne, France

Disclosures: Florian Camy: None; Mousa Mobarki: None; Michel Peoc'H: None; Georgia Karpathiou: None

Background: Immunotherapy targeting the programmed cell death-1/programmed death ligand 1 (PD-L1) pathway has shown promising antitumor activity in brain metastases (BMs).

Since only limited data exist for all various human brain metastases, we aimed to characterize tumor infiltrating lymphocytes (TILs) and PD-L1 in different types of tumors and to compare them with the paired primary tumors.

Design: In this retrospective study of patients histologically diagnosed with brain metastases, we evaluated by immunohistochemistry the differences of PD-L1 and CD8+ TILs density between primary cancers and their corresponding BMs. Analyses for association with clinic-epidemiological and neuroradiological parameters such as patient survival or tumor size were performed.

Results: We analyzed 233 BMs with 111 paired with primary tumors. PD-L1 expression was concordant between BMs and primary tumors in 75.5% of the cases. The discordance in 24,5% of the cases was not significantly associated with any tumor's or patient's characteristic. CD8 expression was concordant between primary and metastatic tumor in 73.3% and 47.8% of the cases for peri- and intra-tumoral expression, respectively. PD-L1 positivity of the primary tumor was directly associated with the positivity of the metastatic focus (p=0.0002). Brain metastases CD8 lymphocytic response was associated with primary tumors CD8 response (p=0.01). PD-L1 expression was associated with CD8 expression in both primary (p=0.0003 for intra-tumoral and 0.07 for peri-tumoral CD8 expression) and metastatic tumors (p<0.0001 for intra-and peri-tumoral expression), as most PD-L1 expressing tumors were those with intense lymphocytic response. No significant associations of patient survival or brain metastases-free survival with PD-L1 or TILs were observed.

Conclusions: Brain metastasis PD-L1 expression is dependent on primary tumor's characteristics, namely the origin and histological type of the primary tumor and its own PD-L1 status, while is independent of all other metastasis characteristics. In this first large study, we show that primary tumor's PD-L1 status can be predictive of the corresponding brain metastasis PD-L1 status with no need for further histologic material in 75% of the cases. Prognosis of brain metastases is not associated with brain metastases PD-L1 or CD8 expression, while time to brain metastases development is associated with primary tumor's type.

1630 Neuropathological autopsy findings after CD19 CAR-T-cell therapy for diffuse large B-cell lymphoma

Samantha Champion[1], Maria Martinez-Lage[1]
[1]Massachusetts General Hospital, Boston, MA

Disclosures: Samantha Champion: None; Maria Martinez-Lage: None

Background: CAR (chimeric antigen receptor) is a recently approved T-cell therapy against CD19 for B-cell malignancies, associated with toxic side effects including cytokine release syndrome (CRS) and CAR-T related encephalopathy syndrome (CRES). The relationship between CRES and neuropathologic findings is uncertain.

Design: Six patients with a history of diffuse large B-cell lymphoma (DLBCL) and treatment with CD19 CAR-T cells underwent full autopsies with brain evaluation. Multiple brain regions were examined with Luxol blue-H&E, CD3, CD45, CD31, and GFAP immunohistochemistry. These were compared with five age-matched controls without history of lymphoma and a variety of underlying systemic and neurological diseases. Histopathological features including white matter injury, gray matter changes, vascular morphology, and inflammation were assessed.

Results: Five patients were male, the mean age was 68 (range 43-82). Interval times between CAR T-cell infusion and death ranged from 18-70 days (average 30 days). Causes of death were progression of DLBCL in three patients, systemic infection in two, and acute respiratory distress syndrome with diffuse alveolar damage in one. Five exhibited CRS symptoms, and five (non-overlapping) exhibited CRES with three severe CRES (Grade>or=3, Scale of 1-4) and two mild CRES (Grade< 3). There was no significant gross evidence of cerebral edema and brain weights were within normal limits (1120g-1480g). All cases had cortical perivascular retraction, which was present but less prominent in four controls. Perivascular strand-like eosinophilic material was readily identified in all cases and seen in four controls. Most of the cases (5/6) had prominent, congested cortical vessels including small vessels with multiple lumens and prominent endothelial layers, highlighted by CD31. Similar vessels were identified in two controls. Perivascular and intraparenchymal CD3+ T-cells were rarely to moderately present, mainly involving white matter, with a larger number seen in the three severe cases. CD45 showed activated cortical microglial cells with certain perivascular predilection. GFAP showed patchy cortical gliosis in most cases but was more marked in the severe cases, involving deeper cortical layers.

Conclusions: Neuropathological autopsy findings in CAR-T cell related neurotoxicity patients are relatively minor morphologically, and include cortical vascular changes, increased white matter CD3+ T-cells, and subpial gliosis which is correlated with the severity of CRES.

1631 Comprehensive Characterization of NT5E/CD73 Expression in Human CNS Neoplasms Reveals Frequent Expression in Gliomas and Meningiomas and Associations with Genotype and Outcome

Shannon Coy[1], Mehdi Touat[2], Jaeho Hwang[3], Patrick Wen[2], Keith Ligon[4], Sandro Santagata[4]
[1]Brigham and Women's Hospital, Harvard Medical School, Boston, MA, [2]Dana-Farber Cancer Institute, Boston, MA, [3]Harvard Medical School, Boston, MA, [4]Brigham and Women's Hospital, Boston, MA

Disclosures: Shannon Coy: None; Mehdi Touat: *Advisory Board Member*, Agios Pharmaceuticals; *Consultant*, Taiho Oncology; *Grant or Research Support*, Merck Sharp and Dohme; Jaeho Hwang: None; Patrick Wen: None; Keith Ligon: None; Sandro Santagata: *Consultant*, RareCyte, Inc.

Background: NT5E/CD73 is the rate-limiting enzyme in catabolism of extracellular ATP or AMP to adenosine. Adenosine levels are often elevated in the tumor microenvironment and suppress anti-tumor immunity via T and NK cell inhibition and upregulation of Tregs, Th17 cells, and type-II macrophages. Elevated CD73 expression is present in numerous cancers and correlates with poor prognosis, metastasis, and drug resistance. CD73 inhibition has shown promising results in pre-clinical trials and promotes cell death and drug sensitization in cultured GBM cells. However, CD73 expression has not been systematically assessed in human CNS neoplasms.

Design: Tissue microarrays were prepared from formalin-fixed paraffin-embedded tissue, including 6 normal brains, 22 pilocytic astrocytomas (PA), 29 ependymomas (EP), 15 anaplastic ependymomas (AEP), 25 medulloblastomas (MED), 133 meningiomas (MEN), 70 atypical meningiomas (AMEN), 20 anaplastic meningiomas (ANMEN), 14 oligodendrogliomas (OLIG), 15 anaplastic oligodendrogliomas (AOLIG), and 280 glioblastomas (GBM). CD73 IHC was performed and membrane staining was assessed with a semi-quantitative scoring system (0-3). *MGMT* promoter methylation, copy-number analysis, DNA sequencing, and outcome data were correlated with CD73 expression. GBM RNA-seq datasets (TCGA, LGG, Ivy-Gap) were analyzed for *CD73* expression.

Results: Normal brains typically showed diffuse moderate CD73 expression in neuropil and vessels. Medulloblastomas were uniformly negative. Ependymomas were typically low or negative (mean±S.D.; 0.5±0.7), and most anaplastic ependymomas were negative (0.1±0.2). PA showed moderate CD73 (1.8±0.7). Grade I meningiomas of all subtypes had high CD73 (2.8±0.5), with lower levels in atypical (2.1±0.9; $p<0.0001$) and anaplastic (1.9±1.0; $p<0.0001$) tumors. GBM (1.9±1.0) and oligodendrogliomas (2.1±1.0) showed varied levels of CD73 by IHC and RNA-seq (**Fig 1**). There was no correlation between CD73 and *MGMT* promoter status. High CD73 correlated

with *EGFR* amplification (p=0.03) in GBM. There was a shorter progression-free survival in IDH-WT GBM with higher CD73 (>1) by IHC (n=58, p=0.048) (**Fig 2**).

Diagnosis	N	Score				Mean
		0	1	2	3	
Normal Brain	6	0	0	5	1	2.2
Pilocytic Astrocytoma	22	0	5	12	5	1.8
Ependymoma	29	13	13	2	1	0.5
Anaplastic Ependymoma	15	12	3	0	0	0.1
Meningioma (Grade I)	133	2	4	11	116	2.8
Atypical Meningioma (Grade II)	70	6	8	28	29	2.1
Anaplastic Meningioma (Grade III)	20	2	4	8	6	1.9
Oligodendroglioma	14	1	2	4	7	2.1
Anaplastic Oligodendroglioma	15	0	5	3	7	2.3
Glioblastoma	280	29	61	90	100	1.9
IDH-Wild Type	259	22	55	87	95	1.9
IDH-Mutant	21	7	6	3	5	1.2
Medulloblastoma	25	25	0	0	0	0

Figure 1 - 1631

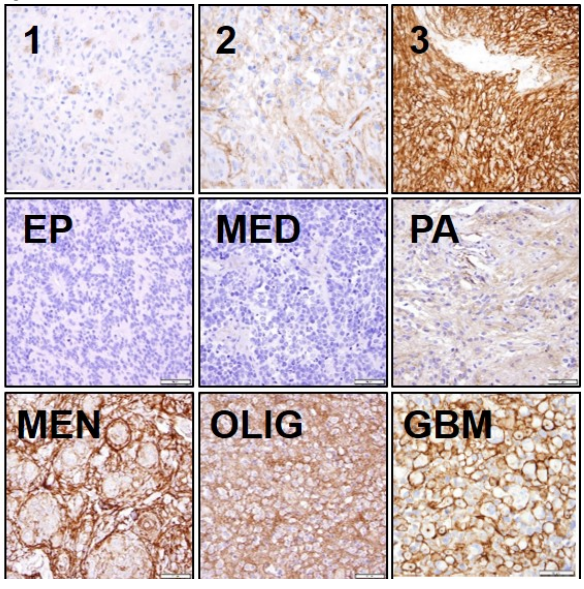

Figure 2 - 1631

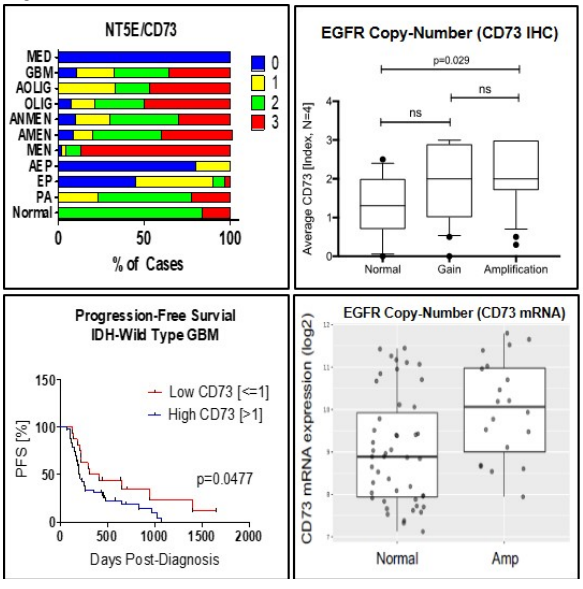

Conclusions: CD73 exhibits distinct expression patterns in human CNS neoplasms, with elevated expression in multiple subtypes. High CD73 expression correlates with poor prognosis and *EGFR* amplification in IDH-WT GBM. These results suggest that CD73 may be a promising prognostic biomarker and therapeutic target in human CNS neoplasms, particularly diffuse gliomas and meningiomas.

1632 Novel TDP-43 Neuropathology in Retinas from Chronic Traumatic Encephalopathy: A Retrospective Analysis of 8 CTE Stage IV Cases

Christina Di Loreto[1], Vanessa Goodwill[2], Donald Pizzo[2], Christina Sigurdson[3], Victor Alvarez[4], Ann McKee[5], Jonathan Lin[6]
[1]Las Vegas, NV, [2]University of California, San Diego, San Diego, CA, [3]University of California, San Diego, La Jolla, CA, [4]Bedford VA Medical Center, Bedford, MA, [5]Boston University, Boston, MA, [6]La Jolla, CA

Disclosures: Christina Di Loreto: None; Vanessa Goodwill: None; Jonathan Lin: None

Background: Chronic traumatic encephalopathy (CTE) is a progressive neurodegenerative disease associated with repetitive mild brain trauma. Clinical features of CTE include behaviorial and mood changes (e.g. irritability, impulsivity, aggression, depression, heightened suicidality), memory impairment, dementia, gait abnormalities and parkinsonism. Visual symptoms are also a complaint in some patients with CTE. While the distinctive brain accumulation of hyperphosphorylated tau and TDP-43 has been elucidated, the neuropathology of CTE in the eyes is unknown. In this study, we evaluated retinal neuropathology from 8 enucleations collected from patients with autopsy-confirmed CTE.

Design: Eight patients (ages 62-93; 8 male) with clinical histories of repetitive brain injury and brain autopsy findings consistent with CTE stage IV were identified. All had athletic histories in contact sports, ranging from amateur to professional. Eight control patients (ages 61-81; 6 male and 2 female) were identified from hospital autopsies. None demonstrated neuropathologic features of CTE at postmortem brain examination. Enucleations were collected from all cases. Pupil-optic nerve cross sections were obtained and stained with hematoxylin and eosin (H&E) and phosphorylated TDP-43 (pTDP-43) by immunohistochemistry.

Results: Retinal thickness was comparable between CTE and control eyes, indicating no overt retinal neurodegeneration in CTE. Strong perinuclear and neuritic and pTDP-43 staining was commonly found in the retinas of CTE eyes (7/8 cases) but rarely seen in control eyes (1/8). The pTDP-43 staining was predominantly confined to a discrete subset of inner nuclear layer interneurons of the retina.

Conclusions: Our findings suggest that CTE is associated with novel retinal neuropathology. Specifically, pTDP-43 is strongly expressed within retinas of CTE eyes in a discrete subset of interneurons of the retinal inner nuclear layer. Interestingly, retinal neuropathology in CTE is not associated with retinal neurodegeneration. We speculate that the retinal neuropathology found in CTE retinas could underlie the visual symptoms reported by CTE patients.

1633 Signaling Pathways of Uveal Melanoma: Exploring New Prognostic Biomarkers

Maria-Carme Dinares[1], Javier Hernandez-Losa[2], Teresa Moline[3], Francisco Casas[4], Atanasio Pandiella[5], Santiago Ramon Y Cajal[6]
[1]Vall d'Hebron University Hospital, Barcelona, Spain, [2]1. Hospital Universitari Vall d'Hebron. 2. VHIR. 3. CIBERONC, Barcelona, Spain, [3]VHIR, Barcelona, Spain, [4]Dexeus University Hospital, Barcelona, Spain, [5]Centro de Investigación del Cáncer, Salamanca, Spain, [6]Vall d'Hebron University Hospital, Barcelona, Catalonia, Spain

Disclosures: Maria-Carme Dinares: None; Javier Hernandez-Losa: None; Teresa Moline: None; Francisco Casas: None; Atanasio Pandiella: None; Santiago Ramon Y Cajal: None

Background: Uveal melanoma (UM) is a little known tumor due to its low incidence, which makes it difficult to study in large series of cases, and where the study of new prognostic markers becomes necessary. The proteins involved in the signaling pathways of MAPK and AKT-mTOR could be found to be deregulated in UM as well as in cutaneous melanoma.

Design: The aim of this work is to study the main signaling pathways of MAPK and AKT-mTOR as well as cell cycle markers in a retrospective series of 101 uveal melanoma patients and finally to correlate the results with clinical-pathological data and follow-up of the patients to explore whether the markers studied can be prognostic.

101 cases of formalin-fixed paraffin-embeded tissue from UMs were retrospectively collected from the archives of two different institutions and stained for pERK1/2, p4EBP1, Ki67 and P16 (whole section) and HER3 (tissue micro array). pERK1/2, p4EBP1, P16 and HER3 were evaluated on the basis of intensity of expression and classified in four categories: 0 (null), 1 (mild), 2 (moderate) and 3 (intense). Ki67 was evalualted on the basis of counting the number of stained nuclei in a high power field.

Results: Low-moderate expression of P16 and Ki67 >22% independently predict disease mortality during follow-up. The risk of death from disease during follow-up is 2.4 times higher in patients with Ki67 >22% than in those with Ki67 <22%. In patients with a low-moderate expression of P16 this risk is 3.1 times higher in patients with a low expression of P16. Combining the 2 markers, the risk of death by disease increases, being 3.6 times higher when both are positive with respect to the rest of patients. (HR: 3.593; 95% CI: 1.465-8.810).

On the other hand, the analysis of HER3 shows that low levels of expression predict an increased risk of developing metastases during follow-up (p=0.035). The study of MAPK and 4E-BP1 was not significant in our series.

	P16 low-moderate (A)	Ki67 >22 nucleous/HPF (B)	Combination A + B
PPV	43,2%	53,3%	77,8%
NPV	85,2%	73,2%	74,2%

Conclusions: Disease-free survival is much lower in those patients in whom the combination of the 2 markers (Ki67 and P16) is positive, being only 33.3% during 10 years of follow-up, compared to 63.8% when only one is positive and 79.1% when both are negative.

HER3 acts as an independent predictive factor in our series.

1634 Histologic, Immunohistochemical, and Molecular Overlaps among Primary and Metastatic Neoplasms in the Central Nervous System of Adults: Potential Pitfalls

Deepak Donthi[1], Stuart Lee[2], Richard Dalyai[2], Keith Tucci[2], Philip Boyer[3]
[1]Vidant Medical Center/East Carolina University, Greenville, NC, [2]Vidant Medical Center, Greenville, NC, [3]East Carolina University, Greenville, NC

Disclosures: Deepak Donthi: None; Stuart Lee: None; Philip Boyer: None

Background: The histologic distinction between primary and metastatic neoplasms in the central nervous system of adults is usually straightforward. Most primary adult neoplasms are astrocytomas or oligodendrogliomas and have an infiltrative growth pattern in neuroparenchyma while most metastatic neoplasms manifest a pushing margin with gliotic neuroparenchyma. This distinction can be challenging when primary or metastatic neoplasms contain a small round blue cell component.

Design: Clinical, imaging, and pathology findings from five cases of central nervous system neoplasm with histologic, immunohistochemical, and/or molecular overlap were compiled over a one-year period. Lymphomas were excluded from consideration.

Results: Cases included a small cell glioblastoma, a glioblastoma with primitive neuronal component, a medulloblastoma, a metastatic small cell carcinoma, and a metastatic non-pigmented melanoma. Histologic overlap included cells with small cell features with scant cytoplasm and a high nuclear to cytoplasmic ratio, nuclear juxtaposition and moulding, and striking perivascular orientation and spread with invasion of neuropil. Immunohistochemical evaluation revealed variable expression of CD56 in all five neoplasms, TTF1 expression in the metastatic small cell carcinoma and both glioblastoma cases (Leica anti-TTF-1 antibody SPT24), and GFAP expression in the glioblastoma and the medulloblastoma cases. Molecular overlap included TERT promoter mutation in the two glioblastoma cases and the medulloblastoma case.

Conclusions: Primary and metastatic neoplasms in the brain can have remarkable histologic overlap creating challenges at the time of frozen section evaluation and during sign-out. Adult medulloblastomas and metastatic small round blue cell neoplasms including lung small cell carcinoma and melanoma can show striking perivascular and to some extent parenchymal invasion that mimics glial neoplasm. Likewise, consideration of a metastatic disease process is evoked by the presence of small cell or primitive neuronal components in astrocytomas and by the rare adult medulloblastoma. Distinguishing primary from metastatic disease can be complicated by (1) variable expression of specific antigens including CD56 and TTF1 and (2) expression of TERT promoter mutation in both glial neoplasms (oligodendrogliomas, primary glioblastomas) as well as adult medulloblastomas. The pathologist must be aware of these overlaps to avoid errant diagnostic conclusions.

1635 Hierarchal Clustering of Immune Checkpoint Gene Expression in Uveal Melanoma from the Cancer Genome Atlas Reveals Distinct Expression Classes that are Associated to Lymphocytic Infiltration, Prognostic Factors, and Progression-Free Survival

Philippe Echelard[1], Leonardo Lando[2], Anne Xuan-Lan Nguyen[3], José-Mario Capo-Chichi[4], Vincent Quoc-Huy Trinh[5]
[1]Université de Sherbrooke, Sherbrooke, QC, [2]Federal University of Goias, Goiania, GO, Brazil, [3]McGill University, Montreal, QC, [4]University Health Network, University of Toronto, Toronto, ON, [5]Centre Hospitalier de l'University de Montreal, Montreal, QC

Disclosures: Philippe Echelard: None; Leonardo Lando: None; Anne Xuan-Lan Nguyen: None; José-Mario Capo-Chichi: None; Vincent Quoc-Huy Trinh: None

Background: Immune checkpoint (IC) inhibition trials are underway for uveal melanoma (UM), yet a clear analysis of the biology and histologic correlates underlying their response is warranted. In this study, we explored The Cancer Genome Atlas (TCGA) dataset for IC gene expression and correlated them with clinical, pathological, outcomes, and molecular data.

Design: Eighty UM are available from TCGA. Known IC genes were selected from Pubmed-cited publications from 2010-2018. Clinical, pathological, histological, and molecular data were extracted using different programs in R and from web-based platforms: R x64 3.5.1,

cBioPortal, TCGABiolinks 3.7, GDC Legacy Archive, GDC Data Transfer Tool v1.3.0. Hierarchal clustering of IC genes Z-scores was performed in Morpheus (Broad Institute) with complete linkage and Euclidian distance. Immune activation classes were selected by clustering. TCGA coded data, pathology reports, and digital diagnostic slides were reassessed by three observes (at least one pathologist), and data was aggregated. All data forms were tested stratified according to IC classes at univariate analyses. Progression-free survival according to classes were also assessed with Kaplan-Meier curves and log-rank testing. Statistics were performed in SPSS v23.0 and TCGABiolinks 3.7.

Results: Hierarchal clustering identified easily distinguishable clusters, classified as Checkpoint-High, Intermediate, Low, and Low with CD40/VTCN1 overexpression (figure 1). Unclassified patients were grouped together. Notably, PD-L1, PD-L2, and CTLA4 were over-expressed in the High and Intermediate classes. Association with different factors show significant lymphocyte expression in Checkpoint-High and Intermediate classes (P=0.000000125) (table 1). Microvascular loops, epithelioid histology, BAP1 mutations, chromosome 3 loss, and chromosome 8 gain were also more frequent in high and intermediate classes. IC classes were significantly stratified at log-rank testing for PFS (figure 2, P=0.001).

TABLE 1. Clinical, histological and molecular characteristics of immune checkpoint classes after hierarchal clustering of related immune gene expression in uveal melanoma from the Cancer Genome Atlas dataset, that achieved **P-value <0.05 at univariate testing**.

	Checkpoint-High (n=7)	**Checkpoint-Intermediate (n=9)**	**Checkpoint-Low (n=38)**	**Checkpoint-Low with CD40/VTCN1(n=15)**	**Others (n=11)**	**p***
Lymphocytes per 6.08 mm^2	0 (0%)	3 (33%)	24 (63%)	5 (33%)	3 (27%)	**$1.25x10^{-7}$**
<40	1 (14%)	3 (33%)	13 (34%)	10 (67%)	7 (64%)	
40-399	6 (86%)	3 (33%)	1 (3%)	0 (0%)	1 (9%)	
>400						
Spindle predominant	0 (0%)	0 (0%)	15 (40%)	10 (67%)	5 (46%)	**0.027**
Mixed	4 (57%)	4 (44%)	14 (37%)	2 (13%)	1 (9%)	
Epithelioid predominant	7 (43%)	5 (56%)	9 (24%)	2 (13%)	2 (18%)	
Prognosis	4 (57%)	3 (33%)	16 (42%)	0 (0%)	3 (27%)	**0.028**
BAP1	0 (0%)	1 (11%)	4 (11%)	5 (33%)	0 (0%)	0.070
EIF1AX	0 (0%)	0 (0%)	12 (32%)	5 (33%)	1 (9%)	0.072
SF3B1						
CHR 1 loss	0 (0%)	0 (0%)	7 (18%)	2 (13%)	0 (0%)	0.245
CHR 3 loss	5 (71%)	6 (67%)	13 (34%)	1 (7%)	5 (46%)	**0.010**
CHR 6 gain	3 (43%)	1 (11%)	9 (24%)	6 (40%)	4 (36%)	0.439
CHR 8 gain	6 (86%)	5 (56%)	14 (37%)	1 (7%)	6 (55%)	**0.005**

*Pearson Chi-Square, Anova test. Median age, personal cancer history, clinical stage, TNM stage, size, extension, mitosis, vascular loops, driver mutation, mean fraction of genome altered, mean mutations in genome were not significant.

Figure 1 - 1635

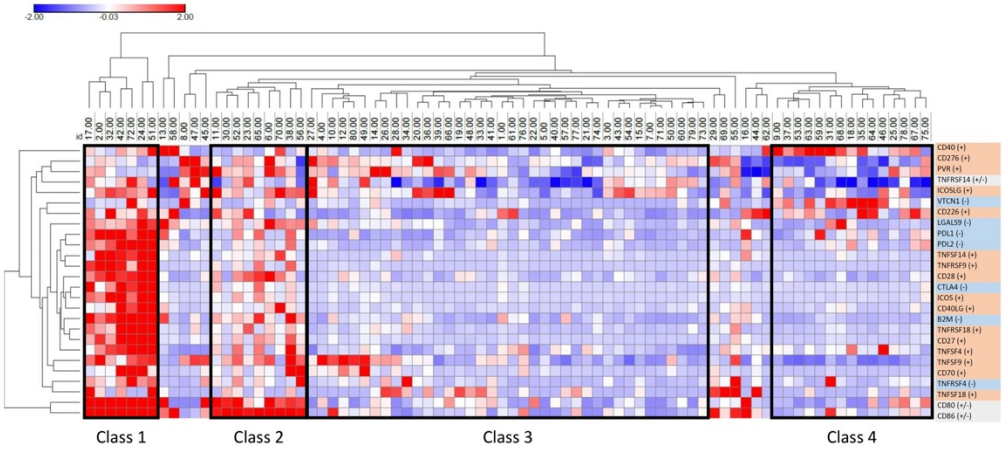

Figure 1. Hierarchal clustering of known tumor-expressed immune checkpoint genes in uveal melanoma from the TCGA dataset, complete linkage, Euclidian distance (Morpheus). We classified tumors into 4 classes. Class 1 (Checkpoint-High) shows strong and consistant overexpression. Class 2 (Checkpoint-Intermediate) shows heightened expression, but less than Class 1. Class 3 (Checkpoint-Low) shows neutral expression. Class 4 (Checkpoint-Low, CD40/VTCN1+) also shows neutral expression, with overexpression of CD40 and VTCN1.

Figure 2 - 1635

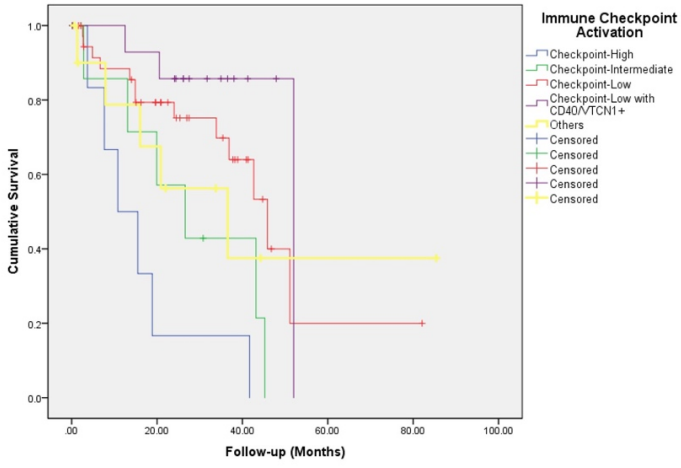

Figure 2. Progression-free survival Kaplan-Meier curves of patients with uveal melanoma from the TCGA according to our immune checkpoint activation classes (log-rank P=0.001).

Conclusions: Hierarchal clustering of IC genes expression identifies at least 4 distinct classes based on IC gene expression, which are significantly associated to histological factors associated to poor prognosis. These classes were also significantly associated to PFS, as higher IC activity is associated to poor prognosis. Additional testing are underway. If validated, these results might underlie the novel treatment biomarkers for current immunotherapy trials in parallel to PD-L1 immunohistochemical testing.

1636 Characterization of Cancer Immune Profiles in Patients with Primary Central Nervous System Lymphoma

Fei Fei[1], Al Amri Raniah[1], Deniz Peker[2]
[1]The University of Alabama at Birmingham, Birmingham, AL, [2]University of Alabama at Birmingham, Birmingham, AL

Disclosures: Fei Fei: None; Al Amri Raniah: None; Deniz Peker: *Advisory Board Member*, Abbvie

Background: Primary central nervous system lymphoma (PCNSL) is a rare and aggressive extranodal variant of non-Hodgkin lymphomas with disease limited to the brain, spinal cord, leptomeninges or eyes, without evidence of systemic involvement. PCNSL has a poor prognosis with a median overall survival of 30-50 months. Recently, correlation of tumor microenvironment and limited immune surveillance on the lymphoma pathogenesis and survival has been recognized, however, little is known about PCNSL. The aim of this study is to characterize the cancer immune profiles in patients with PCNSL and associate the findings with clinical outcome.

Design: Twelve archival FFPE specimens from PCNSL patients between 2005 and 2017, along with clinical information were collected. Total RNA was extracted and the PanCancer IO 360 panel (NanoString Technologies) was used to assess the expression of 770 immune response genes in tumor tissues from the PCNSL patients. Data analysis was performed using nSolver software and the Advanced Analysis Module (NanoString Technologies).

Results: The male:female ratio was 5:7, the median age was 64 years (range: 31-84 years) and the median overall survival (OS) was 3.5 months (range: 1-36 months). Twelve patients were divided into short OS group (OS <=3.5 month, n=7) and long OS group (OS > 3.5 months, n=5). The gene expression profiles of long OS group versus short OS group were analyzed and statistically significant up-regulation of 32 genes and down-regulation of 13 genes were identified as shown in Table 1. The clusters were enriched for the genes related to antigen presentation, costimulatory signaling, immune cell adhesion and migration, interferon signaling, JAK-STAT signaling, cytotoxicity and lymphoid compartment. Furthermore, cell type profiling analysis revealing cytotoxic cells, macrophages, neutrophils, T cells, CD8+ cells and Th1 cells were highly correlated with PCNSL ($p < 0.05$) as shown in Figure 1.

Table 1. Differential gene expresison in primary central nervous system lymphoma patients (n=12) from long overall survival group vs short overall survival group.

Gene Name	Log2 Fold Change	Std Error (log2)	Lower Confidence Limit (log2)	Upper Confidence Limit (log2)	p-value
HLA-DPA1	1.54	0.2	1.15	1.94	1.57E-05
HLA-DPB1	1.8	0.353	1.11	2.49	0.000464
HLA-DQB1	-5.77	1.13	-7.99	-3.54	0.000476
HLA-DQA1	-8.73	1.74	-12.1	-5.32	0.000527
HLA-DRA	1.86	0.392	1.09	2.63	0.000777
HLA-DOA	1.46	0.308	0.854	2.06	8.00E-04
TLR9	-1.47	0.42	-2.29	-0.646	0.00575
FAM30A	-4.06	1.17	-6.35	-1.77	0.006
PDCD1LG2	1.26	0.409	0.461	2.06	0.0115
TNFRSF9	2.03	0.657	0.74	3.32	0.0115
THY1	1.63	0.534	0.585	2.68	0.0121
HSD11B1	1.65	0.549	0.576	2.73	0.0131
STAT4	2.22	0.742	0.762	3.67	0.0136
SOCS1	1.72	0.58	0.585	2.86	0.0141
GPR160	0	0.542	-2.66	-0.535	0.0146
KLRB1	3.03	1.04	1	5.07	0.0152
IDO1	1.97	0.673	0.649	3.29	0.0152
GBP4	1.44	0.503	0.454	2.42	0.0168
CSF1R	1.36	0.48	0.422	2.31	0.0176
CTLA4	2.04	0.731	0.605	3.47	0.0192
CDH11	1.2	0.435	0.344	2.05	0.0204
COL11A1	1.87	0.687	0.522	3.22	0.0216
SYK	-1.28	0.473	-2.21	-0.352	0.0222
HLA-DOB	1.94	0.726	0.52	3.37	0.0232
PLA1A	1.78	0.668	0.473	3.09	0.0236
CXCL9	2.27	0.862	0.578	3.96	0.0251
CD2	1.17	0.448	0.296	2.05	0.0255
CXCL13	2.7	1.03	0.681	4.72	0.0255
NECTIN1	-1.13	0.441	-2	-0.27	0.0278
HLA-DMB	0.824	0.321	0.196	1.45	0.0279
ALDOC	-1.19	0.462	-2.09	-0.281	0.028
PTEN	-0.497	0.201	-0.892	-0.103	0.0332
TNFRSF18	1.96	0.808	0.378	3.54	0.0356
FOXP3-mRN	2.26	0.93	0.435	4.08	0.0356
MAML2	-0.95	0.392	-1.72	-0.182	0.0359
HLA-E	0.919	0.392	0.15	1.69	0.0412
GAS1	2.12	0.913	0.334	3.91	0.0423
CXCL14	2.33	1	0.367	4.3	0.0423
FAM124B	0.574	0.247	0.089	1.06	0.0428
CD36	-1.84	0.801	-3.41	-0.271	0.0444
ANLN	-0.837	0.365	-1.55	-0.12	0.0451
OASL	2.04	0.896	0.283	3.8	0.0461
CCNE1	-0.843	0.371	-1.57	-0.116	0.0463
CXCL12	1.6	0.708	0.215	2.99	0.047
ELOB	-0.693	0.309	-1.3	-0.0879	0.0486

Figure 1 - 1636
Figure 1. Cell type score from primary central nervous system lymphoma (PCNSL) patients (n=12) .

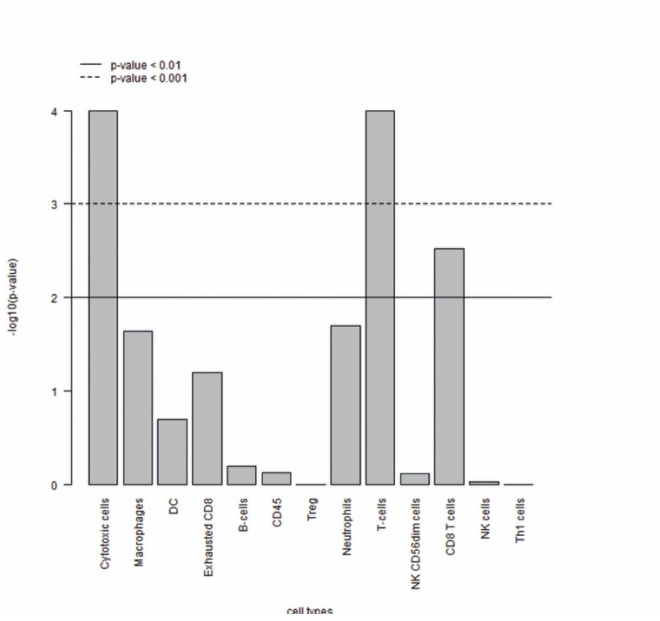

Conclusions: Our data reveals a distinct PCNSL tumor microenvironment and immune responses. Characterization of cancer immune profiles in PCNSL patients could be used to predict clinical outcome of patients. However, these findings need to be further validated in a larger population.

1637 Mutations of the MAPK/TSC/mTOR pathway characterize periventricular glioblastoma with epithelioid SEGA-like morphology – implications for therapy

Maria-Magdalena Georgescu[1], Yan Li[2], Adriana Olar[3], Gregory Fuller[4]
[1]Louisiana State University/Shreveport, Shreveport, LA, [2]LSU Health Shreveport, Shreveport, LA, [3]Medical University of South Carolina, Charleston, SC, [4]The University of Texas MD Anderson Cancer Center, Houston, TX

Disclosures: Maria-Magdalena Georgescu: None; Yan Li: None; Adriana Olar: None; Gregory Fuller: None

Background: Glioblastoma is the most frequent and aggressive glial tumor in adults, with an incidence of 3-4 cases per 100 000 population, and a median survival of 1.3 years. Because of its dismal prognosis, an intense search for new therapies has been linked to an effort to discover new therapeutic targets. In glioblastoma, stratification criteria by morphological-molecular correlations are now sought after at the time of the initial diagnosis in order to inform timely therapeutic decisions with critical implications for patient survival. Epithelioid glioblastoma is a recognized glioblastoma variant, recently added to the brain tumor classification, with similar prognosis as the classic variant, and B-Raf V600E mutations in 50% of the cases.

Design: We identified a new subset of epithelioid glioblastoma with periventricular location and subependymal giant cell astrocytoma (SEGA)-like morphology. The clinical history, including therapy and survival, magnetic resonance imaging, histology and genomic profiling by NGS and SNP-microarray are provided for three patients with four temporally different specimens.

Results: Genomic profiling of the tumors showed either driver mutations in *NF1* and *MTOR*, or subclonal mutation in *TSC1*, indicating upregulation of the MAPK/TSC1/mTOR pathway. *TSC1* and *MTOR* mutations have been previously described in low grade glioma, such as SEGA, or focal cortical dysplasia, respectively. Unlike these, the mutations from SEGA-like glioblastoma occurred in the context of other genetic aberrations seen in high grade neoplasms, including in *CDKN2A/B*, *EGFR*and *PIK3CA*. For one patient with two temporally distinct specimens, the subclonal *TSC1* pathogenic mutation was detected only in the specimen showing SEGA-like appearance, indicating requirement for strong mTOR activation as trigger for this specific epithelioid/SEGA-like morphology. Our findings also reveal drug actionable mutations, as FDA-approved kinase inhibitors are available at many steps of the MAPK/mTOR pathway.

Conclusions: The recognition of this new subset of periventricular high grade gliomas with clear phenotypic-genotypic correlates is essential for prompt marker testing and therapeutic management of these patients and advocates for the therapeutic targeting of the MAPK/TSC/mTOR pathway for these high grade epithelioid gliomas that may otherwise behave aggressively when treated only with conventional therapy.

1638 Mutation status, epithelial differentiation and location stratify risk for tumor recurrence in chordoid meningioma

Maria-Magdalena Georgescu[1], Yan Li[2], Adriana Olar[3], Bret Mobley[4], Phyllis Faust[5], Jack Raisanen[6]
[1]Louisiana State University/Shreveport, Shreveport, LA, [2]LSU Health Shreveport, Shreveport, LA, [3]Medical University of South Carolina, Charleston, SC, [4]Vanderbilt University, Nashville, TN, [5]Columbia University, New York, NY, [6]University of Texas Southwestern, Dallas, TX

Disclosures: Maria-Magdalena Georgescu: None; Yan Li: None; Adriana Olar: None; Bret Mobley: None; Phyllis Faust: None; Jack Raisanen: None

Background: Meningiomas are heterogenous tumors and their pathologic classification in the WHO Classification of Tumors of the CNS comprises 13 recognized histologic variants. Chordoid meningioma is a rare and more aggressive histologic variant of meningioma. Due to paucity of cases, the molecular profiling and patient risk stratification were not addressed in this variant.

Design: In this study, we performed an integrated clinical, NHERF1 immunohistochemical (IHC) and next generation sequencing (NGS) analysis of WHO grade II chordoid meningiomas from 30 patients (34 cases), representing the largest study to date. The NGS was performed in Dr. Georgescu's laboratory, by using a 295-gene library containing genes with recurrent mutations in adult and pediatric, primary and metastatic brain cancer. The DNA library was generated at Agilent with 97-100% gene coverage, based on hybrid-capture/target-enrichment SureSelect XT HS technology that yields high QC values and good on-target rates.

Results: The patients with chordoid meningioma have demographic characteristics different from the general population: younger age of onset (45 vs 65), skull base location for the female patients (6:1), and increased recurrence rate (30% at 5 years). NHERF1 microlumen extent directly correlated with skull base location and segregated tumors into three cell differentiation categories –fibroblastic (13.3%), epithelial/poorly-differentiated (26.7%) and epithelial/well-differentiated (60%). NGS identified *NF2* and *TRAF7*, as the most common mutated genes, correlating with the location and epithelial differentiation of the tumors. Mutations in *AKT1*, *KLF4* and *MN1* were found in isolated well-differentiated skull base tumors. Mutations in genes not previously involved in meningioma pathogenesis were also found, with *SLC9A3R2*, *RDX* and *ERRFI1* mutations identified in two or more tumors. The integrated tumor analysis stratified the patients into a high recurrence risk population, characterized by tumors harboring *NF2* mutations and poor epithelial differentiation, and a low recurrence risk population, characterized by tumors exhibiting either epithelial differentiation, skull base location and *TRAF7/AKT1/KLF4* mutations, or fibroblastic differentiation, non-skull base location and other mutations.

Conclusions: This is the first study of the integrated mutational landscape of chordoid glioma with important implications for patient risk stratification and management.

1639 Mismatch Repair Mutations in Pediatric Glioblastoma

Catherine Gestrich[1], Marta Couce[2], Navid Sadri[3], Mark Cohen[4], Robin Elliott[1]
[1]University Hospitals Cleveland Medical Center, Case Western Reserve University, Cleveland, OH, [2]UH Cleveland Medical Center, Cleveland, OH, [3]Cleveland, OH, [4]University Hospitals of Cleveland, National Prion Disease Pathology Surveillance Center, Highland Heights, OH

Disclosures: Catherine Gestrich: None; Marta Couce: None; Navid Sadri: None; Mark Cohen: None; Robin Elliott: None

Background: Glioblastoma (GBM) is the most frequent cause of cancer related death among children with an overall median survival of 9-15 months. A significant proportion of pediatric GBMs occur within the context of cancer predisposition syndromes, and demonstrate molecular profiles distinct from those seen in adults. A high percentage of pediatric GBMs demonstrate mismatch reapir deficiency, especially in geographic locations with high consanguinity. These tumors have a high tumor mutation burden, which may result in neoantigen expression and sensitivity to immune checkpoint inhibitors. The aim of this study was to investigate the prevalence of MMR deficency amoung our pediatric GBMs in comparison to our IDH-mutant and IDH-WT adult GBMs.

Design: We selected a total of 22 GBM cases; 11 pediatric and 11 adult (6 IDH-mutant and 5 IDH-WT). A tissue microarray was constructed with all cases in duplicate, 1.5 mm cores. IHC for MLH1, MSH2, PMS2 and MSH6 was performed. DNA and RNA was extracted from FFPE tumor samples and used for library preparation with Life Technologies Oncomine Comprehensive V3 assay. Next-generation sequencing was performed with Ion Torrent sequencer and post-sequencing mutational analysis was performed using Ion Reporter software.

Results: We detected genomic alterations in all pediatric cases with an average of 3.5 alterations per sample. The most frequently mutated gene was TP53 (54.5%, 6/11). H3F3A was mutated in 27% (3/11) of samples, all of which were the K28M variant. We also found alterations in several of the MMR genes in 27% (3/11) of the samples, which correlated with loss of IHC staining. The latter also correlated with samples that had the highest tumor mutational burden. In the adult cohort, genomic alterations were detected in 91% (10/11) of samples with an average of 2.5 alterations per sample. None of the adult cases demonstrated MMR defects.

Conclusions: Next-generation sequencing, in combination with routine IHC, can provide essential diagnostic, prognostic and therapeutic information for these patients. As expected, the pediatric and adult GBMs from our catchment area differ in their genetic profile. In addition, the detection of alterations in MMR genes in a signifcant number of pediatric cases in combination with the potential therapeutic benefits resulting from such mutations, emphasizes the need to incorporate MMR testing in the routine diagnostic work up for these patients.

1640 Morphometric Comparison of Retinal vs Brain PrP Aggregates in 14 Cases of Sporadic Creutzfeldt-Jakob Disease

Vanessa Goodwill[1], Christina Sigurdson[2], Jonathan Lin[3]
[1]University of California, San Diego, San Diego, CA, [2]University of California, San Diego, La Jolla, CA, [3]La Jolla, CA

Disclosures: Vanessa Goodwill: None; Christina Sigurdson: *Advisory Board Member*, Amydis; Jonathan Lin: None

Background: Prion diseases are a rare group of diseases leading to rapid cognitive decline. Up to 50% of patients with prion disease develop visual symptoms. A growing number of studies reveal the presence of abnormal prion protein (PrP^{Sc}) deposits in the retinas of patients with sporadic Creutzfeldt-Jakob Disease (sCJD). Molecular, histologic, and functional differences between retinal and brain PrP^{Sc} deposits are unknown. Here, we performed detailed histologic measurements of retinal PrP^{Sc} deposits from 14 clinically documented sCJD cases for comparison to brain PrP^{Sc} deposits.

Design: From December 2015 to May 2017, 28 eyes were collected from 14 autopsies of clinically suspected prion disease and 6 of non-prion controls. sCJD was confirmed concomitantly by brain autopsy. Immunohistochemistry was performed with antibodies against PrP and deposition within the retina was evaluated. We measured 202 retinal PrP deposits across 14 sCJD cases and 202 brain PrP deposits across the cerebral cortex and thalamus in a case of sCJD. Statistical significance was evaluated using an unpaired t-test and Mann-Whitney test.

Results: In all fourteen CJD cases, PrP^{Sc} deposits are observed in the retina as discrete puncta confined to the inner and outer plexiform layers. No retinal deposits were observed in control cases. Comparatively, brain deposits in sCJD are widespread. PrP^{Sc} deposits are significantly smaller in the retina than brain (5.02 um +/- 0.50 vs 36.78 um +/- 34.55, $p<0.0001$). The retinal deposits show consistent globular morphology, in stark contrast to the highly variable dot-to-fibrillar morphology of brain deposits. Retinal PrP deposits were not associated with retinal spongiosis or degeneration, while brain PrP^{Sc} deposits are consistently associated with severe spongiotic neurodegeneration.

Conclusions: PrP^{Sc} deposits are a consistent finding in the retinas of patients with prion disease. These retinal PrP deposits adopt completely different morphologic features compared to corresponding brain deposits. The retinal deposits are consistently localized in discrete retinal lamina that we speculate correspond to photoreceptor synaptic boutons. Retinal PrP deposition does not appear to be linked to neurodegeneration within the neuroretina, in contrast to the severe spongiotic neurodegeneration induced by brain PrP deposits. Investigating how the neuroretina survives and tolerates PrP^{Sc} deposits may provide insight into how neuronal cells cope with PrP^{Sc}.

1641 Adult Glioblastoma and the role of Daxx (Death domain associated protein 6) tumor biomarker

Sean Hacking[1], Mansoor Nasim[2], Deepika Savant[3], Cao Jin[4], Seungjun Ahn[5]
[1]Northwell Health, Queens, NY, [2]Northwell, Lake Success, NY, [3]Northwell Health, Lake Success, NY, [4]Donald and Barbara Zucker School of Medicine at Hofstra/Northwell, Lake Success, NY, [5]Feinstein Institute for Medical Research, Great Neck, NY

Disclosures: Sean Hacking: None; Mansoor Nasim: None; Deepika Savant: None; Cao Jin: None; Seungjun Ahn: None

Background: Glioblastoma, also known as glioblastoma multiforme (GBM), is the most aggressive cancer that begins within the brain. Patients with GBM have a poor prognosis and only 3–5% of them survive for more than 5 years. This study is a retrospective study of the histopathology and the biomarker expression of the patients who were diagnosed with GBM at our health system. We included 72 cases of GBM, where we sought to determine if DAXX (A protein which functions to regulate apoptosis) was associated with both patient survival time, and tumor size.

Design: Tissue microarrays (TMA) were constructed from the 72 GBM cases, each containing duplicate tissue cores of 1 or 1.5 mm diameter sampled from the most representative areas of the donor blocks. Immunohistochemical antibody for DAXX-1 was used to determine protein expression. Factors including tumor size and survival status were compared to different cohorts of DAXX-1 expression; limited expression <25%, and definite expression (>25%). We quantified staining into nuclear, cytoplasmic, membranous, and overall staining pattern. The Kaplan-Meier product limit method was used to estimate the survival time in days from date of diagnosis, in order to compare survival time with the groups (< 25% vs. > 25%). The two-sample t-test was utilized to compare tumor size (largest dimension) at diagnosis between groups (< 25% vs. > 25%).

Results: Of the 72 cases the overall staining pattern showed that 33 tumors had definite expression of DAXX, and 39 had limited expression. It is worth noting that we found a spectrum of staining, nuclear staining being the most prominent. Importantly we found

that patient's with tumors that had less than 25% immunohistochemical staining for DAXX-1 had A statistically significant larger tumor size compared to patients with greater than 25% (Mean (SD) = 3.79 (1.64) vs. 2.76 (1.67), p < 0.010). The estimated median time to survival for patients who had less than 25% staining was 385 days, and for patients who had greater than or equal to 25% staining was 466 days. Patients with definite expression of DAXX lived and average of 81 days longer, however this was not statistically significant (p<0.876).

Figure 1 - 1641

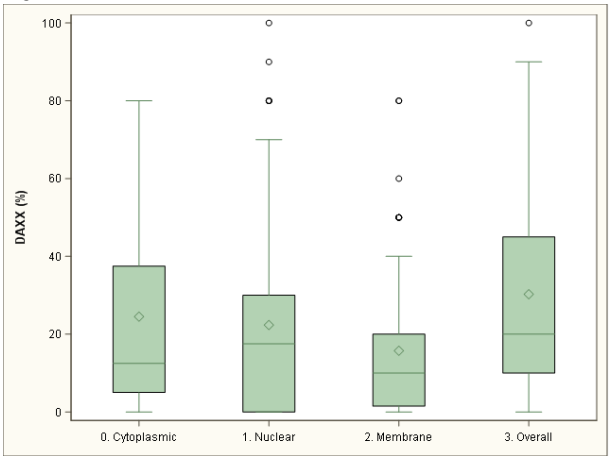

Figure 2 - 1641

Analysis of Variance for Variable tumor size
Classified by Variable overall Daxx staining cohort

Overall Daxx Staining	N	Mean
0. < 25%	39	3.792308
1. >= 25%	33	2.757576

Conclusions: In conclusion limited DAXX expression is associated with larger GBM tumors, and shorter survival time (not statistically significant). This may suggest that DAXX plays an important role in tumorogenesis. Such findings may have significant implications on target therapies and surgical decision making for patients with GBM.

1642 Density of Cerebral Microbleeds is Independent of Severity of Alzheimer's Disease and Cerebral Amyloid Angiopathy, a Neuropathological Study

Alyssa Higgins[1], Elizabeth Davaro[1], Miguel Guzman[1]
[1]Saint Louis University, St. Louis, MO

Disclosures: Alyssa Higgins: None; Elizabeth Davaro: None; Miguel Guzman: None

Background: Cerebral microbleeds (CMB) are small perivascular hemosiderin deposits that are considered biological markers of cerebral small vessel disease. Prior studies of CMB have focused on characteristic radiographic findings with few having neuropathologic correlation. CMB have been associated with cognitive impairment and cerebrovascular disease, however their clinical significance and implications are unknown. Recent studies have shown high prevalence of CMB in Cerebral Amyloid Angiopathy (CAA), a condition that is associated with aging and AD. Literature on CMB and severity of Alzheimer's Disease (AD) is scarce. We investigated the prevalence and association of CMB with AD and CAA.

Design: A single institution retrospective review was performed from 2010 to 2018 and a cohort of Saint Louis University Brain Bank specimens was established. Patients were selected based on established criteria: age greater than 60, post-mortem diagnosis of AD, and availability of slides representing required areas of the brain. Sections from five different areas of each brain were examined: cortex, subcortical white matter, basal ganglia, midbrain, and brainstem. Blinded evaluation was performed independently by three reviewers. Twenty vessels were randomly selected from each evaluated region and the number of hemosiderin deposits recorded. The number and location of the CMB were then correlated with the patient's probability of AD based on the "ABC" score as established by the National Institute on Aging and Alzheimer's Association (NIA-AA) guidelines.

Results: A total of 37 patients (mean age 82.2 years) with a clinical history of cognitive impairment and post-mortem diagnosis of AD were selected. Patient demographics: 15 males (41%) with a mean age 76.9 years; 22 females (59%) with a mean age 76.5 years. AD neuropathology scoring was as follows: low 9 patients (24.3%); intermediate 18 patients (48.6%); high 10 patients (27%). CAA was present in 19 patients (51.4%). All patients demonstrated CMB in all five regions with the highest density in: white matter, followed by brainstem, cortex, basal ganglia, then midbrain. There was no significant difference between the number of CMB and presence of CAA, or "ABC" score for AD.

Figure 1 - 1642

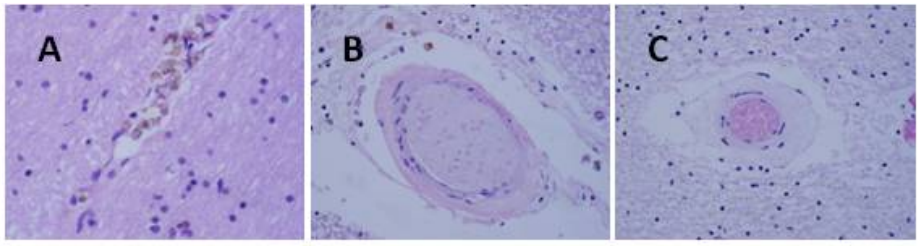

Figure 1: (A) Cerebral microbleeds pictured in the peri-vascular space of a white matter blood vessel. Cerebral Amyloid Angiopathy with (B) and without (C) cerebral microbleeds.

Conclusions: Despite previous imaging based study results, we did not find an association between the presence of CAA and number of CMB. In patients with a post-mortem diagnosis of AD, CMB are a common independant finding unrelated to the severity of neuropathological changes.

1643 BAP1 Immunostain for Uveal Melanoma in Fine-Needle Aspiration Biopsy Specimens Highly Correlates with Other Prognostic Markers

Cristiane Ida[1], Jose Pulido[2], Patricia Greipp[2], Joaquin Garcia[2], Timothy Olsen[2], Diva Salomao[2]
[1]Rochester, MN, [2]Mayo Clinic, Rochester, MN

Disclosures: Cristiane Ida: None; Jose Pulido: None; Patricia Greipp: None; Joaquin Garcia: None; Timothy Olsen: None; Diva Salomao: None

Background: Loss of BAP1 protein expression has emerged as a negative prognostic marker in uveal melanoma (UM). Fine-needle aspiration biopsy (FNAB), a relatively safe procedure used to obtain material for diagnosis and ancillary studies, has gained popularity as part of the management of patients with UM.

Design: We retrospectively evaluated BAP1 immunostaining in 17 FNAB specimens and 8 subsequent enucleations. Results were correlated with clinical and follow-up data, chromosome 3 status by FISH (monosomy vs. disomy) (n=7) and UM-specific gene expression profile (GEP; n= 11, 6 also had FISH).

Results: There were 6 females and 11males, with median age at diagnosis of 61 years (range, 46-83) and UM involving the right eye in 9 patients. FNAB was performed to obtain tissue for prognostication prior to brachytherapy (n=12) or diagnostic confirmation (n=5), mostly using a 25-gauge needle (n=12; range, 20-30), and it was diagnostic in all cases. Of the 17 patients undergoing FNAB, 13 received brachytherapy, 5 followed by enucleation, and 4 were treated with enucleation only. BAP1 nuclear immunostaining was positive in 10, negative in 4 and equivocal in 3 FNAB specimens. When positive, BAP1 immunostaining was diffuse (>90% tumor nuclei) in most cases. BAP1 immunostaining results were concordant between all FNAB and subsequent enucleation specimens. Among the 3 FNAB cases with equivocal results, BAP1 was positive in 2 enucleations and negative in one. A positive BAP1 result on FNAB correlated with disomy 3 (n=4) and GEP class 1 (n=6). A negative BAP1 result on FNAB correlated with monosomy 3 (n=2) and GEP class 2 (n=2). FISH and GEP were not available in 5 cases. Median follow-up was 52 months for all patients (range, 3-133). Among BAP1-negative patients, 4 were alive without disease (at 11, 14, 51 and 124 months postoperatively) and one died with metastatic disease. In patients with BAP1-positive UM, 8 were alive without disease and 4 died (two with metastatic disease, one without disease and one with unknown disease status).

Conclusions: In conclusion, BAP1 immunostaining in FNAB specimens shows high concordance with well-established prognostic markers for UM and with results in subsequent enucleation specimens, representing an alternative/additional prognostic tool. BAP1 immunostaining interpretation on FNAB specimens is relatively easy but it can be challenging in a small subset of cases due to low cellularity and difficulty in distinguishing positivity in neoplastic versus non-neoplastic cells.

1644 The Misclassification of Diffuse Gliomas: National Rates and Outcomes

J. Bryan Iorgulescu[1], Matthew Torre[2], Maya Harary[3], Timothy Smith[3], David Reardon[4], Jill Barnholtz-Sloan[5], Arie Perry[6]
[1]Boston, MA, [2]Brigham and Women's Hospital, Harvard Medical School, Brookline, MA, [3]Brigham and Women's Hospital, Harvard Medical School, Boston, MA, [4]Dana-Farber Cancer Institute, Boston, MA, [5]Case Western Reserve University, Cleveland, OH, [6]University of California, San Francisco, San Francisco, CA

Disclosures: J. Bryan Iorgulescu: None; Matthew Torre: None; Maya Harary: None; Timothy Smith: None; Jill Barnholtz-Sloan: None; Arie Perry: None

Background: The integrated histopathological and molecular diagnoses of the 2016 WHO classification of CNS tumors have revolutionized patient care by improving diagnostic accuracy and reproducibility; however, the frequency and consequences of misclassification in historical cohorts of diffuse gliomas diagnosed by histology alone (i.e. prior WHO classification schema) are unknown.

Design: Patients with newly-diagnosed ICD-O3 histologically-encoded diffuse gliomas from 2010-2015 were identified from the National Cancer Database (NCDB), which comprises >70% of all cancers newly-diagnosed in the U.S. The outcomes were the misclassification rates of diffuse glioma by WHO grade and 1p/19q molecular status, compared to ICD-O3 histology coding, and assessed by ANOVA or χ^2 test. The associated OS was assessed by Kaplan-Meier and log-rank techniques.

Results: 74,718 patients with newly-diagnosed diffuse gliomas were identified, including 91.8% and 10.7% with recorded WHO grade and 1p/19q status, respectively. The WHO grade of histologically-encoded gliomas was concordant in 65.7% and 86.3% of diffuse (grade II) astrocytomas and oligodendrogliomas, 90.4% and 90.0% of anaplastic (grade III) astrocytomas and oligodendrogliomas, and 98.7% of glioblastomas (grade IV). Only 74.4% and 78.8% of molecularly characterized WHO grade II and III oligodendrogliomas, respectively, were in fact, 1p/19q-codeleted. Additionally, 28.9% and 36.8% of histologically-encoded WHO grade II and III "oligoastrocytomas", and 6.3% and 8.8% of WHO grade II and III astrocytomas had 1p/19q-codeletion, thus molecularly representing oligodendrogliomas if also IDH-mutant. OS significantly depended on accurate WHO grading and 1p/19q status.

Discordance between ICD-O-3 Histological Diagnosis and 1p/19q-codeletion Status in Diffuse Gliomas

WHO grade	ICD-O-3 Histology	Have 1p/19q data (n)	1p/19q-codeleted			Age (years)			Male		Frontal lobe		Overall Survival (months)		
				n	%	Median	IQR	*p-value**	%	*p-value***	%	*p-value***	5yr-OS	95% CI	*p-value****
II	**Diffuse OG**	1,345	Yes	1,001	74.4	39	(29-49)	***<0.001***	57.6	*0.44*	74.8	***<0.001***	90.9	(87.4-93.4)	***0.01***
			No	344	25.6	42	(33-51)		55.2		58.2		84.9	(78.6-89.5)	
	Diffuse AC	544	Yes	34	6.3	36	(29-46)	*0.43*	52.9	*0.77*	57.7	*0.72*	81.4	(57.5-92.6)	*0.85*
			No	510	93.8	39	(29-51)		55.5		53.7		70.6	(62.1-77.6)	
	Mixed Glioma	564	Yes	163	28.9	35	(29-45)	***0.001***	46.6	***0.003***	76.5	***<0.001***	83.8	(75.0-89.7)	*0.09*
			No	401	71.1	43	(32-51)		60.4		58.8		74.7	(67.8-80.3)	
III	**Anaplastic OG**	664	Yes	523	78.8	44	(32-58)	***0.05***	59.9	*0.95*	76.9	***0.001***	78.5	(72.5-83.2)	***<0.001***
			No	141	21.2	48	(38-57)		59.6		62.9		48.6	(35.4-60.6)	
	Anaplastic AC	815	Yes	72	8.8	42	(31-56)	*0.10*	47.2	*0.23*	51.0	*0.10*	53.7	(34.5-69.6)	*0.86*
			No	743	91.2	47	(33-57)		54.6		52.9		48.5	(42.6-54.1)	
	Mixed Glioma	456	Yes	168	36.8	41	(31-55)	*0.39*	52.4	*0.13*	74.2	*0.17*	72.6	(63.5-79.8)	***0.004***
			No	288	63.2	44	(33-55)		59.7		63.9		56.8	(49.4-63.4)	
IV	**Glioblastoma**	2,427	Yes	227	9.4	60	(52-69)	***0.03***	63.9	*0.05*	43.4	*0.66*	18.1	(10.5-27.4)	***0.01***
			No	2,220	91.5	59	(49-68)		57.1		38.7		10.9	(8.70-13.4)	

OG: oligodendroglioma, AC: astrocytoma, IQR: interquartile range, OS: overall survival, CI: confidence interval; *p-value from a t-test; **p-value from a chi-square test; *** p-value from a log-rank test using Kaplan-Meier survival analysis

Conclusions: Many diffuse gliomas have been misclassified in the NCDB, with significant clinical implications. Our findings suggest that when including historical histologically-classified cohorts for comparison, there is the potential for false-positive results in contemporary therapeutic trials of molecularly-classified diffuse gliomas. These issues may be true for institutional historical databases, as well as

registry-based sources, and could contribute to a seemingly positive phase II trial (based on historical comparison) failing at the phase III stage. Critically, findings from diffuse glioma clinical trials and historical cohorts using prior WHO schemes based on histology alone must be cautiously re-interpreted.

1645 The Feasibility of Relying on Next Generation Sequencing to Diagnose Gliomas

Kwok Ling Kam[1], Christina Appin[2], Qinwen Mao[3], Sachie Ikegami[4], Somak Roy[5], Daniel Brat[1], Craig Horbinski[6], Marina Nikiforova[5]
[1]Northwestern University Feinberg School of Medicine, Chicago, IL, [2]Northwestern University, Chicago, IL, [3]Northwestern Medicine, Chicago, IL, [4]University of Chicago, Chicago, IL, [5]University of Pittsburgh Medical Center, Pittsburgh, PA,[6]Chicago, IL

Disclosures: Kwok Ling Kam: None; Christina Appin: None; Qinwen Mao: None; Sachie Ikegami: None; Somak Roy: None; Daniel Brat: None; Craig Horbinski: None; Marina Nikiforova: None

Background: Advanced molecular diagnostics has become a routine part of the molecular workup of gliomas, as it has consistently proven more reliable at classification and prognostication than traditional light microscopy. The power and widespread use of next-generation sequencing (NGS), in which multiple high-yield genes and hotspots are simultaneously interrogated, has raised questions as to whether it could supplant histologic-based examination in surgical neuropathology. We therefore sought to determine the feasibility of relying on NGS for pathologic diagnosis, without the benefit of histology.

Design: Neuropathologic cases of brain lesions in adults (18+ years old), all of which had been analyzed by GlioSeq NGS, comprised the study cohort (N=183). Twelve cases showed no molecular alterations, leaving 171 with interpretable results. Each case was separately scored by 6 reviewers, representing a wide range of expertise. Reviewers were asked to render their best diagnoses, including WHO grade, based solely on age, sex, tumor location, and NGS results. Results were compared to the final integrated reports, and scored on the following scale: 0=either wrong tumor type (e.g. astrocytoma versus oligodendroglioma), or correct tumor type but off by 2+ grades; 1=off by 1 grade; 2=exactly correct. Histology alone was treated as a seventh reviewer.

Results: Overall reviewer scores ranged from 81.6-94.2%, closely matching expertise in brain tumor molecular diagnostics. Histology alone scored 87.1%, with the most common “error” being under-grading of a glioblastoma due to a lack of histologic features. Among diffusely infiltrative gliomas, reviewers had the highest accuracy in diagnosing glioblastoma (95.8%), but accuracy in grade II-III astrocytomas and oligodendrogliomas was much worse (59-79%). Accuracy was only 52% in BRAF V600E tumors, which contained a variety of tumor types. Of the 12 cases in which NGS was negative, 8 were histologically recognizable as tumors, ranging from craniopharyngioma and pilocytic astrocytoma to recurrent glioblastoma with reactive gliosis.

Conclusions: It is not possible to reliably diagnose gliomas and other brain tumors based exclusively on NGS, especially in distinguishing between grade II-III astrocytomas and oligodendrogliomas. However, it is also no longer possible to diagnose and classify gliomas based only on histologic features. A combination of both modalities is essential in order to provide the best possible patient care.

1646 Observations of the Morphological Evolution of Neuronal Intranuclear Rods in the Human Substantia Nigra Across the Age Spectrum

Osama Khan[1], Mario Capitano[1], Xin Yan Fan[2], Anthea Paul[2], John Woulfe[2], Jean Michaud[1]
[1]University of Ottawa, Ottawa, ON, [2]The Ottawa Hospital - University of Ottawa, Ottawa, ON

Disclosures: Osama Khan: None; Mario Capitano: None; Xin Yan Fan: None; Anthea Paul: None; John Woulfe: None; Jean Michaud: None

Background: Parkinson's disease (PD) is a neurodegenerative disease characterized by a depletion of dopaminergic neurons in the substansia nigra (SN). Loss of SN neurons occurs at a rate of up to 10% per decade in non-pathological ageing. Other age-related changes in nigral neurons include accumulation of intranuclear inclusions called Marinesco Bodies (MBs). MBs have been shown to associate with a distinct type of neuronal intranuclear body called the intranuclear rod (INR). At what point in the ageing process INRs develop, and when they give rise to MBs, are questions that remain unanswered. In this observational study, we set out to determine whether SN INRs display changes in their morphology across the human age spectrum.

Design: The laboratory information system was searched for hospital and forensic autopsies conducted from 2010-2017 that had midbrain sections taken. Ten slides were cut from each of 11 age groups from ages ranging from 1 month to 80 years of age. Sections were immunostained with glucocorticoid receptor (GR) to identify INRs.

Results: There was a progressive age-associated transition in INR morphology from long, linear intranuclear structures in the youngest age groups (infants), to shorter linear structures at middle ages, culminating in small, dot-like juxtanucleolar structures in elderly subjects. A proportion of short INRs displayed contact with MBs in the middle age groups.

Age	Gender	Diagnosis
1 month	M	Not Known
2 month	F	Not Known
20 year old	M	Acute Hypoxic Encephalopathy
23 year old	F	Leigh Syndrome
44 year old	F	Normal
46 year old	F	Normal
60 year old	F	Acute Hypoxic Encephalopathy
60 year old	M	Alzheimers Disease
80 year old	M	Mild Hypoxic Encephalopathy
80 year old	F	Large Hemorrhagic Stroke, Cerebral Infarct

Figure 1 - 1646

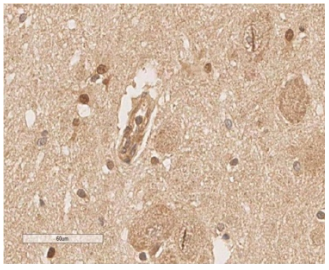

Figure 2 - 1646

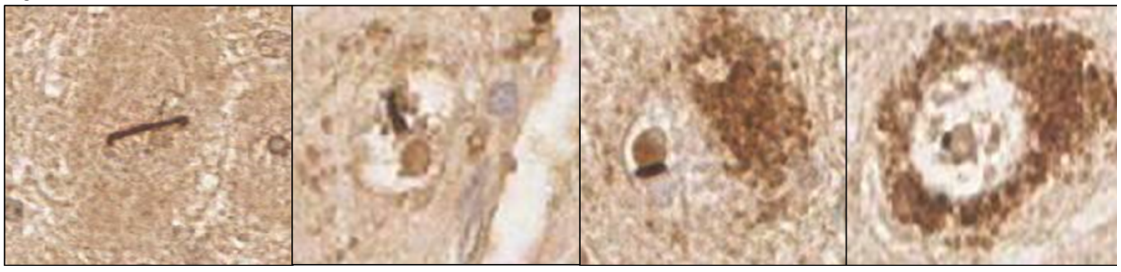

Conclusions: We demonstrated a striking progressive, age-dependent alteration in INR morphology. These results suggest that INRs give rise to MBs in the SN during middle ages. As a follow-up of this preliminary observational study, quantitative analysis of INR frequency and size is currently being performed in our lab. Ultimately, we plan to expand our cases for the creation of a human SN tissue microarray which we hope will shed light on the cellular mechanisms of neuronal ageing and degeneration in the SN.

1647 E Cadherin mRNA and IHC Expression in Subtypes of Corticotroph Adenomas

Bette Kleinschmidt-DeMasters[1], Margaret Wierman[2], Katja Kiseljak-Vassiliades[2]
[1]University of Colorado Anschutz Medical Campus, Aurora, CO, [2]University of Colorado, Aurora, CO

Disclosures: Bette Kleinschmidt-DeMasters: None; Margaret Wierman: None; Katja Kiseljak-Vassiliades: None

Background: We (Endocrine 2015;49(1):231-41), and others, have shown that subtyping of growth hormone (GH) adenomas correlates with behavior and response to therapies. One of the major immunohistochemical (IHC) markers that differentiate aggressively-behaving sparsely granulated GH adenomas from more indolent, densely granulated GH adenomas (along with numerous keratin+ fibrous bodies) is the loss of expression of E-cadherin in the former, but not the latter. Distinction between GH adenoma subtypes has clinical utility since sparsely granulated GH adenomas are less responsive to somatostatin analog therapy. As such, since 2015, we have routinely performed E-cadherin IHC on all pituitary adenomas and have observed that the only other pituitary adenoma type with variability in E-cadherin expression is corticotroph (ACTH) adenomas. We wondered whether 1.) E cadherin was variable at the mRNA level in any adenoma type, 2.) E-cadherin mRNA level might correlate with clinical secretory status, and 3.) E cadherin IHC might supplement subtyping into sparsely versus densely granulated ACTH+ tumors.

Design: Databases were searched for pituitary adenomas, 1/1/2015-9/14/2018. Affymetrix microarray for mRNA expression for E-cadherin (CHD1) was conducted on 94 fresh frozen samples of pituitary adenomas of varying types removed at the time of surgery, as described (Endocrinology 2017;158(5):1450-1460). For ACTH+ adenomas, patient charts were retrospectively assessed for clinically-active versus -silent features. IHC results were reviewed.

Results: mRNA expression levels for E-cadherin in GH adenomas showed strong tendency for stratification by subtype (Figure 1). ACTH+ adenomas were the only other adenomas to show a significant range in E-cadherin mRNA levels, confirming our IHC experience; no correlation was found between mRNA level and clinical activity. Review identified 21 sparsely /35 densely granulated ACTH+ adenomas, with strong versus weak/absent E cadherin IHC ratios of 17:4 in sparsely granulated and 16:19 in densely granulated. Thus, unlike GH adenomas, there was no 1:1 correlation between granulation subtype and E cadherin expression in ACTH+ adenomas, or loss of E cadherin IHC and increased invasiveness in ACTH+ adenomas (Figure 2).

Figure 1 - 1647

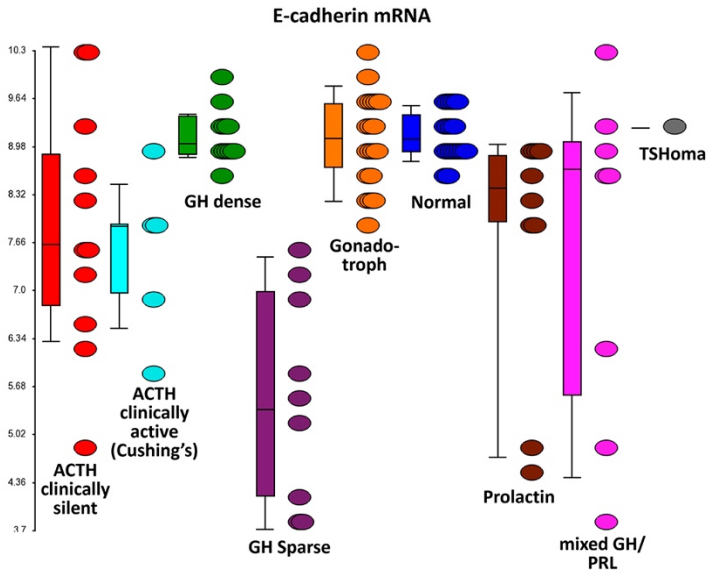

Figure 2 - 1647

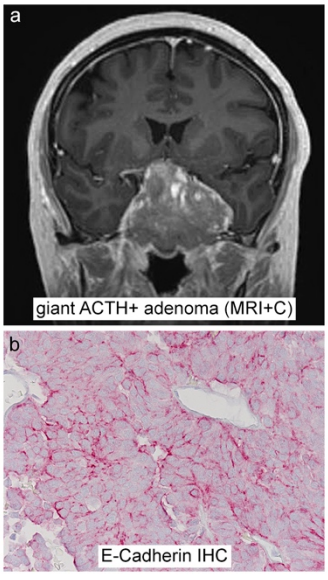

Conclusions: E-cadherin IHC cannot supplement subtyping of ACTH+ adenomas, does not correlate with clinically-active versus clinically-silent status, and does not show 1:1 correlation with invasiveness.

1648 Histo-Genomic Review of Digital Diagnostic Slides from the Cancer Genome Reveals Differentially Expressed Cellular Pigmentation Genes that are Correlated to Uveal Melanoma Pigmentation Intensity and its Association to Poor Prognosis Factors and Progression-Free Survival

Leonardo Lando[1], Philippe Echelard[2], Anne Xuan-Lan Nguyen[3], José-Mario Capo-Chichi[4], Vincent Quoc-Huy Trinh[5]
[1]Federal University of Goias, Goiania, GO, Brazil, [2]Université de Sherbrooke, Sherbrooke, QC, [3]McGill University, Montreal, QC, [4]University Health Network, University of Toronto, Toronto, ON, [5]Centre Hospitalier de l'University de Montreal, Montreal, QC

Disclosures: Leonardo Lando: None; Philippe Echelard: None; Anne Xuan-Lan Nguyen: None; José-Mario Capo-Chichi: None; Vincent Quoc-Huy Trinh: None

Background: Pigmentation in oncogenesis is not well understood and has previously been hinted as a factor of poor prognosis in uveal melanoma (UM). Furthermore, no study has studied the biology underlying this association. In this study, we explored histological pigmentation intensity in UM from the Cancer Genome Atlas (TCGA) dataset and focus our analyses on clinical outcomes, pathological and molecular data available.

Design: Eighty UM are available from TCGA. Clinical, pathological, histological, and molecular data were extracted using different software in R and from web-based platforms: R x64 3.5.1, cBioPortal, TCGABiolinks 3.7, GDC Legacy Archive, GDC Data Transfer Tool v1.3.0. Digital diagnostic and frozen section slides were all reviewed by three observers in Aperio Imagescope v12.2.2.2.5015, and 3 groups of pigmentation intensity were defined (Poor 0-4%, Intermediate 5-50%, Rich 51-100%, figure 1), with review of all other pathological findings. Genes involved in cellular pigmentation were selected from the International Federation of Pigment Cell Society, and differential gene expression was tested from normalized data generated by RSEM, using the Z-ratio method with a false discovery rate (FDR)<0.05. Statistics were performed in SPSS v23 and TCGABiolinks 3.7.

Results: The 80 UMs analyzed were divided in groups 1 (N=31), 2 (N=26) and 3 (N=23) according to pigmentation intensities. Pigmentation detected by histological review of digital slides showed average correlation with pathology reports (Spearman R=0.409, P=0.001). At univariate analysis, median age, T stage, EIF1AX mutation, BAP1 mutation, chromosome 3 loss and chromosome 8 gain and rates of mutations in whole-exome sequencing data were significantly associated to pigmentation levels (Table 1). Globally, higher pigmentation is consistently associated to factors of poor prognosis. Progression-free survival (PFS) is illustrated in figure 2, showing reduced survival in pigment-rich tumors (log-rank P=0.047). The MBTPS1, GPR143, CITED1, SLC45A2, TYRP1, PDPK1, NOTCH2, GGT1, SOX18 and ATOX1 pigmentation related genes were differentially expressed and significantly correlated to the percentage of pigmentation at histological review (*FDR*-corrected P=0.0003 to 0.0459).

Table 1. Clinical, pathological, and molecular characteristics of patients with uveal melanoma from the TCGA dataset, stratified by pigmentation intensity.

	Pigment poor (n=31)	Pigment intermediate (n=26)	Pigment rich (n=23)	P
Median age (IQR)	56.0 (47.0-69.0)	59.5 (52.5-72.8)	71.0 (59.5-77.0)	**0.035**
Male sex	17 (55%)	15 (58%)	13 (57%)	0.976
Personal cancer history	1 (3%)	2 (8%)	1 (4%)	0.732
Clinical stage I II III IV	0 (0%) 16 (52%) 14 (45%) 1 (3%)	0 (0%) 9 (36%) 14 (56%) 2 (8%)	0 (0%) 14 (61%) 8 (35%) 1 (4%)	0.494
T stage T1 T2 T3 T4	0 (0%) 8 (26%) 12 (39%) 11 (36%)	0 (0%) 5 (19%) 5 (19%) 16 (62%)	0 (0%) 1 (4%) 15 (65%) 7% (30%)	**0.01**
N stage NX N0 N1	2 (7%) 29 (94%) 0 (0%)	2 (8%) 24 (92%) 0 (0%)	0 (0%) 23 (100%) 0 (0%)	0.418
M stage MX M0 M1	15 (48%) 15 (48%) 1 (3%)	6 (23%) 18 (69%) 2 (8%)	4 (17%) 18 (78%) 1 (4%)	0.112
Size Basal diameter (SD) Thickness (mm) (SD)	14.6 (3.7) 9.8 (3.0)	15.2 (4.1) 11.4 (4.0)	16.0 (2.5) 10.4 (2.8)	0.336 0.286
Extension Extrascleral Optic nerve invasion	0 (0%) 2 (7%)	4 (16%) 0 (0%)	3 (14%) 0 (0%)	0.096 0.196
Mitosis/6.08 mm^2 (SD)	12.5 (10.0)	12.8 (9.5)	11.5 (9.5)	0.891
Lymphocytes/6.08 mm^2 <40 40-399 >40	13 (42%) 16 (52%) 2 (7%)	11 (42%) 9 (35%) 6 (23%)	11 (48%) 9 (39%) 3 (13%)	0.403
Main vascular pattern Silent or classical Straight, parallel, arcs Extensive networks	10 (32%) 17 (55%) 4 (13%)	11 (42%) 9 (35%) 6 (23%)	10 (44%) 10 (44%) 3 (13%)	0.564
Presence of vascular loops	14 (45%)	10 (39%)	9 (39%)	0.851
Histologic variant Spindle predominant Mixed Epithelioid predominant	11 (36%) 13 (42%) 7 (23%)	13 (50%) 9 (35%) 4 (15%)	6 (26%) 7 (30%) 10 (44%)	0.174
Driver mutation GNA11 GNAQ CYSLTR2 Other	13 (42%) 18 (58%) 1 (3%) 1 (3%)	12 (46%) 11 (42%) 1 (4%) 2 (8%)	11 (48%) 11 (48%) 1 (4%) 0 (0%)	0.902 0.481 0.977 0.361
Prognostic mutations BAP1 EIF1AX SF3B1	5 (16%) 7 (23%) 8 (26%)	13 (50%) 3 (12%) 7 (27%)	8 (35%) 0 (0%) 3 (13%)	0.024 **0.045** 0.435
Chromosomal alterations 1 loss 3 loss 6 gain 8 gain	4 (13%) 9 (29%) 11 (36%) 7 (23%)	2 (8%) 7 (27%) 4 (15%) 11 (43%)	3 (13%) 14 (61%) 8 (35%) 14 (61%)	0.783 **0.023** 0.186 **0.017**
Mean fraction of genome altered (SD)	0.1 (0.1)	0.2 (0.1)	0.2 (0.1)	0.491
Mean mutations in genome (SD)	27.4 (68.9)	15.8 (5.2)	15.2 (4.6)	**0.003**

*Kruskal-Wallis, Pearson Chi-Square, Anova test

.

Figure 1 - 1648

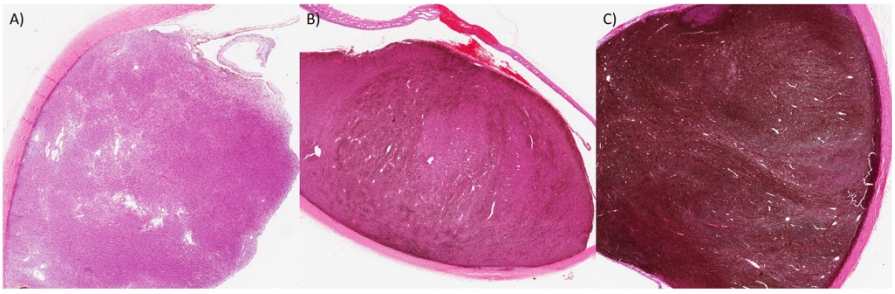

Figure 1. Different degrees of uveal melanoma pigmentation, digital diagnostic slides from the Cancer Genome Atlas, reviewed by three observers (10X magnification). A) Almost complete absence of pigmentation, classed as pigment poor as % of pigmentation is between 0-4%. B) Minor level of pigmentation, classed as pigment intermediate as % of pigmentation is between 5-50%. C) Heavily pigmented tumor, classed as pigment rich as % of pigmentation is between 51-100%.

Figure 2 - 1648

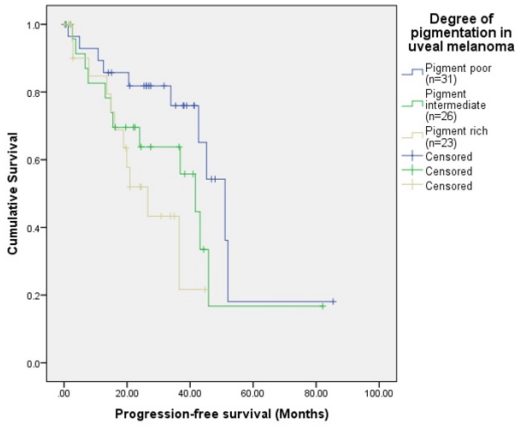

Figure 2. Progression-free survival in uveal melanoma from the Cancer Genome Atlas, according to degree of pigmentation (log-rank P=0.047).

Conclusions: Clinic-pathological results analyzed from the TCGA dataset suggest that a higher degree of pigmentation is correlated to different factors of poor prognosis and worst PFS. Additional gene testing and enrichment analyses are currently underway.

1649 Microvascular Loops and Networks in Uveal Melanoma are Associated to Poor Outcomes Irrespective of Classical Poor Prognosis Factors, and Identification of Differentially Expressed Angiogenesis Genes: Histo-Genomic Analysis of the Cancer Genome Atlas Dataset

Leonardo Lando[1], Philippe Echelard[2], Anne Xuan-Lan Nguyen[3], José-Mario Capo-Chichi[4], Vincent Quoc-Huy Trinh[5]
[1]Federal University of Goias, Goiania, GO, Brazil, [2]Université de Sherbrooke, Sherbrooke, QC, [3]McGill University, Montreal, QC, [4]University Health Network, University of Toronto, Toronto, ON, [5]Centre Hospitalier de l'University de Montreal, Montreal, QC

Disclosures: Leonardo Lando: None; Philippe Echelard: None; Anne Xuan-Lan Nguyen: None; José-Mario Capo-Chichi: None; Vincent Quoc-Huy Trinh: None

Background: Vasculature in uveal melanoma (UM) has been widely studied, and microvascular loops (MVL) and networks are recognized as poor prognosis factors. However, their biological development is not well understood. Furthermore, many clinical trials testing anti-angiogenesis are currently underway, yet none have analyzed the vascular patterns. In this study, we explored histologically detected MVL in UM from the Cancer Genome Atlas (TCGA) and focus our analyses on clinical outcomes, pathological and molecular data available.

Design: Eighty UM are available from TCGA. Clinical, pathological, histological, and molecular data were extracted using different programs in R and from web-based platforms: R x64 3.5.1, cBioPortal, TCGABiolinks 3.7, GDC Legacy Archive, GDC Data Transfer Tool v1.3.0. Digital diagnostic and frozen section slides were reviewed by three observers in Aperio Imagescope v12.2.2.2.5015, and vascular patterns were annotated (figure 1), with review of all other pathological findings. Presence of MVL was noted if either histological review, pathology report or TCGA data noted their presence. Genes associated to tumor angiogenesis (Pubmed-cited reviews, 2010-2018) and in UM (articles, 2010-2018) were selected. Differential gene expressions were tested from normalized data generated by RSEM, using the Z-ratio method with a false discovery rate (FDR)<0.05. Statistics were performed in SPSS v23 and TCGABiolinks 3.7.

Results: 33 of the 80 UMs analyzed showed MVL; univariate analysis detected an association between optic nerve invasion/presence of epithelioid histology and MVL (table 1). Notably, M stage and clinical stage were not associated to MVL. SF3B1 was significantly less frequent in the presence of MVL (table 1). MVL showed higher rates of chromosome 3 loss and 8 gain (table 1). Progress-free survival is illustrated in figure 2, showing worst survival with MVL (log-rank P=0.047). EPHA5, ABCB7, DLD, YAP1, ATM, RAP1B, HIF1A, SSSCA1 and DBT genes (Top 10) were differentially expressed in MVL among the 430 tumoral angiogenesis-related genes analyzed (FDR-corrected P=0.000018-0.008). Of interest, the members of the VEGF family did not show significant differential expression.

Table 1. Clinical, pathological, and molecular characteristics of uveal melanoma from the Cancer Genome Atlas, stratified by the presence of microvsacular loops.

	Absence of microvascular loops (n=47)	Presence of microvsacular loops (n=33)	Total (n=80)	P*
Median age (IQR)	60 (50-75)	64 (54-74.5)	61.5 (51-74.8)	0.335
Male sex	23 (49%)	22 (67%)	45 (56%)	0.169
Personal cancer history	2 (4%)	2 (6%)	4 (5%)	1.000
Clinical stage I II III IV	0 (0%) 24 (51%) 21 (45%) 2 (4%)	0 (0%) 15 (47%) 15 (47%) 2 (6%)	0 (0%) 39 (49.4%) 36 (45.6%) 4 (5.1%)	0.888
T stage T1 T2 T3 T4	0 (0%) 8 (17%) 19 (40%) 20 (43%)	0 (0%) 6 (18%) 13 (39%) 14 (42%)	0 (0%) 14 (17.5%) 32 (40.0%) 34 (42.5%)	0.990
N stage NX N0 N1	2 (4%) 45 (96%) 0 (0%)	2 (6%) 31 (94%) 0 (0%	4 (5.0%) 76 (95.0%) 0 (0%)	1.000
M stage MX M0 M1	11 (23%) 34 (72%) 2 (4%)	14 (42%) 17 (51%) 2 (6%)	25 (31.3%) 51 (63.7%) 4 (5.0%)	0.158
Size Mean basal diameter (mm) (SD) Mean thickness (mm) (SD)	15.1 (3.6) 10.7 (3.2)	32 (15.3) 10.2 (3.4)	15.2 (3.5) 10.5 (3.3)	0.812 0.553
Extension Extrascleral Optic nerve invasion	2 (5%) 2 (5%)	0 (0%) 9 (27%)	7 (9.3%) 2 (2.7%)	0.508 **0.009**
Mean mitosis per 6.08 mm^2(SD)	11.8 (9.3)	13.1 (9.6)	12.3 (9.6)	0.531
Lymphocytes per 6.08 mm^2 <40 40-399 >40	24 (51%) 18 (38%) 5 (11%)	11 (33%) 16 (49%) 6 (18%)	35 (43.8%) 34 (42.5%) 11 (13.8%)	0.263
Mean pigmentation (SD)	33.9 (33.6)	31 (33.2)	32.7 (33.3)	0.700
Hystologic variant Spindle predominant Mixed Epithelioid predominant	25 (53%) 13 (28%) 9 (19%)	5 (15%) 16 (49%) 12 (36%)	30 (38%) 29 (36%) 21 (26%)	**0.002**
Predominant vascular pattern Silent or classical Straight, parallel, arcs Networks (extensive network)	26 (55%) 21 (45%) 0 (0%)	5 (15%) 15 (46%) 13 (39%)	31 (38.8%) 36 (45.0%) 13 (16.3%)	**<0.001**
Driver mutation GNA11 GNAQ CYSLTR2 Other	21 (45%) 25 (53%) 3 (6%) 0 (%)	15 (46%) 15 (46%) 0 (0%) 3 (9%)	36 (45%) 40 (50%) 3 (3.8%) 3 (4%)	1.000 0.650 0.264 0.066
Prognostic mutations BAP1 EIF1AX SF3B1	12 (26%) 7 (15%) 16 (34%)	14 (42%) 3 (9%) 2 (6%)	26 (32%) 10 (13%) 18 (23%)	0.147 0.512 **0.003**
Chromosomal alterations 1 loss 3 loss 6 gain 8 gain	5 (11%) 13 (28%) 15 (32%) 14 (30%)	4 (12%) 17 (52%) 8 (24%) 18 (55%)	9 (11%) 30 (38%) 23 (29%) 32 (40%)	1.000 **0.037** 0.616 **0.037**
Mean fraction of genome altered (SD)	0.1 (0.12)	0.2 (0.12)	1.8 (9.8)	0.370
Mean mutations in genome (SD)	23.8 (55.9)	14.9 (4.4)	0.1 (0.3)	0.401

*Welch's T-test, Mann-Whitney U test, Pearson Chi-Square, Fisher's exact test.

Figure 1 - 1649

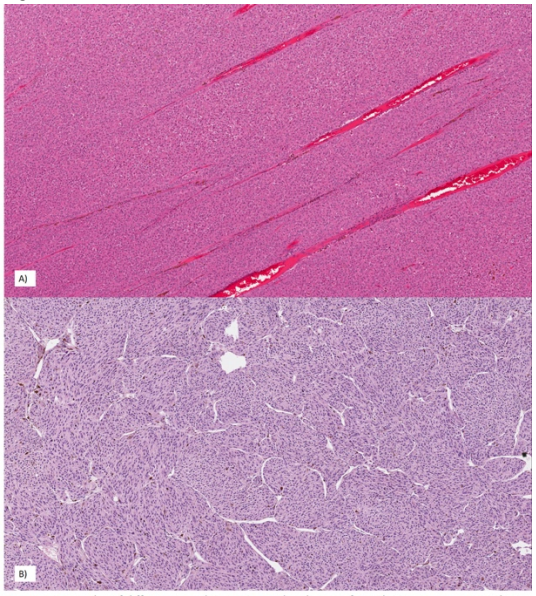

Figure 1. Examples of different vasculatures in uveal melanoma from the Cancer Genome Atlas, with the digital diagnostic slides was reviewed by three observers (100X). The main vascular pattern was first identified, as well as the presence of microvascular loops and networks. A) The vessels are arranged in a parallel pattern without important branching, without the presence of microvascular loops (50X). B) The vessels are connected between each other in semi-arcs, creating islets of tumoral cells as the vessels are closed into three dimensional vsacular loops, here being categorized as vascular networks (50X).

Figure 2 - 1649

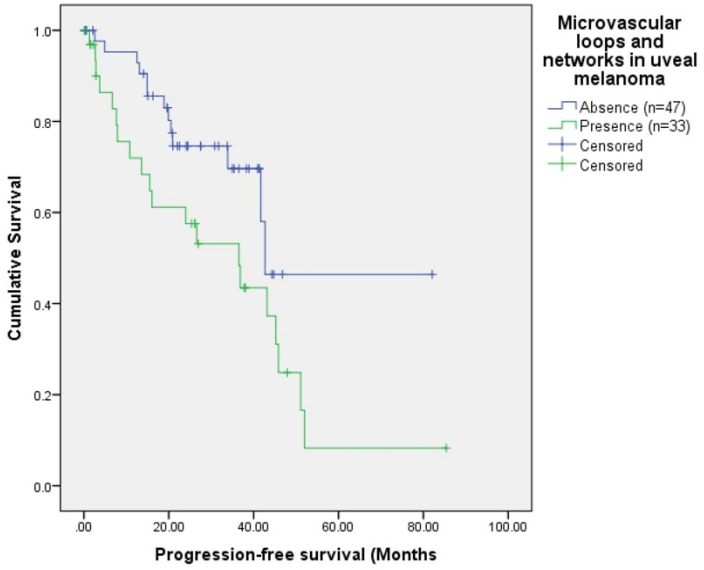

Figure 2. Progression-free survival according to the presence of microvascular loops and networks in uveal melanoma from the Cancer Genome Atlas (log-rank P=0.047).

Conclusions: Clinic-pathological results analyzed from the TCGA dataset are comparable to previous studies, noting the correlation to poor outcomes, yet no strong association with the VEGF family members. These results suggest that alternate pathways exist and are implicated in the development of MVL.

1650 Clinicopathologic Features of Intracranial Desmoplastic Small Round Cell Tumors

Julieann Lee[1], Sean Ferris[1], Elaine Cham[2], Ahmed Gilani[3], Bette Kleinschmidt-DeMasters[4], Dimitri Trembath[5], Manuela Mafra[6], Cheng-Hsuan Chiang[7], David Ellison[8], David Solomon[1], Arie Perry[1]
[1]University of California, San Francisco, San Francisco, CA, [2]UCSF Benioff Children's Hospital Oakland, Oakland, CA, [3]University of Colorado, Denver, CO, [4]University of Colorado Anschutz Medical Campus, Aurora, CO, [5]University of North Carolina, Chapel Hill, NC, [6]The Portuguese Institute of Oncology, Lisbon, Portugal, [7]St. Jude Children's Research Hospital, Memphis, TN, [8]St. Jude Children's Research Hospital, Memphis, TN

Disclosures: Julieann Lee: None; Sean Ferris: None; Dimitri Trembath: None; Cheng-Hsuan Chiang: None; David Ellison: None; David Solomon: None; Arie Perry: None

Background: Desmoplastic small round cell tumors (DSRCT) are malignant mesenchymal neoplasms that typically occur intra-abdominally. They are defined by an EWSR1-WT1 gene fusion and display a polyphenotypic immunoprofile with co-expression of epithelial (keratins, EMA), mesenchymal (desmin), and neuronal (NSE, synaptophysin) markers. To the best of our knowledge, five intracranial DSRCTs have been reported in the literature (PMID: 9263077, 25479120).

Design: We encountered five cases of intracranial DSRCTs. Available clinical, morphologic, immunohistochemical, and genetic features were compiled.

Results: There were 4 male and 1 female patients (age range 6-25 years; median 13 years). Three tumors were supratentorial, while two were located in the posterior fossa. Initial diagnostic impressions included anaplastic medulloblastoma, astroblastoma-like neoplasm, low-grade tumor with glioneuronal features, and malignant tumor NOS. The maximal mitotic index ranged from 1 to 12 (median 6). There was a prominent desmoplastic stroma in three and three contained necrosis. Cases either demonstrated EWSR1-WT1 fusion by sequencing (4/5) or EWSR1 gene rearrangement by break-apart FISH (1/5). There was strong desmin positivity in four tumors with patchy immunoreactivity in one. Of four cases tested for epithelial makers such as EMA, CAM 5.2, and other keratins, there was strong positivity in one, focal positivity in two, and absence of staining in one. There was weak or focal synaptophysin positivity in 4/5 tumors, weak or patchy NeuN staining in 2/2 cases, focal/patchy S100 staining in 4/4 cases, and patchy neurofilament positivity in 1/4 cases.

Conclusions: The morphology of intracranial DSRCT is variable and can include an astroblastoma-like pattern, non-desmoplastic medulloblastoma-like features, and can even appear low-grade. As such, it remains unclear if this represents the same entity as seen

elsewhere in the body. Also, intracranial tumors with EWSR1-WT1 fusion may not always robustly express epithelial lineage markers. Further study of additional cases will assist in recognizing the full clinicopathologic spectrum.

1651 Aberrant Immunophenotype in Meningiomas: Potential Major Diagnostic Pitfalls

Stephanie Livingston[1], Anas Bernieh[2], Siraj El Jamal[3], Ali Saad[4]
[1]University of Tennessee Health Science Center, Memphis, TN, [2]University of Mississippi Medical Center, Jackson, MS, [3]Icahn School of Medicine at Mount Sinai, New York, NY, [4]Methodist/LeBonheur Health System, Memphis, TN

Disclosures: Stephanie Livingston: None; Anas Bernieh: None; Siraj El Jamal: None; Ali Saad: None

Background: Meningiomas are typically characterized by expression of EMA and vimentin. However, aberrant immunophenotypic features which overlap with solitary fibrous tumor (SFT) and less commonly, neurofibroma and schwannoma can be encountered and represent a potential diagnostic pitfall, particularly when the tumor occurs in the cerebello-pontine angle region. We report aberrant immunophenotype in 17 cases of meningiomas.

Design: A total of 17 meningiomas with immunoexpression of CD34 and/or S-100 are collected from multiple institutions. Electron microscopy (EM) was performed on all cases using tissue extracted from paraffin-embedded tissue.

Results: A total of 17 meningiomas (13 females and 4 males-median age: 57.7 years) are retrieved from the files. All meningiomas corresponded to WHO grade I. Eleven meningiomas were CD34-positive. The positivity varied from focal (8 cases) to diffuse (3 cases). Six cases showed strong positivity for S-100 (focal in 3 and diffuse in 3). Two cases showed dual positivity for CD34 and S-100 in a focal but strong immunostaining pattern. Of the 11 CD34-positive meningiomas, EMA was diffusely positive in 4, focally positive in 5, and negative in 2. Of the 6 S-100-positive meningiomas, EMA was diffusely positive in 2, focally positive in 3, and negative in one. In both cases with dual immunoexpression of CD34 and S-100, EMA was completely negative. In 7 cases of CD34-positive meningiomas foci reminiscent of SFT, including loose proliferation of spindle cells embedded within a fibrous stroma and vague hemangiopericytoma-like vasculature, were present. This was particularly true in the fibrous type. All CD34-positive tumors were negative for STAT6. In all S-100-positive tumors, no areas corresponding to verocay bodies, commonly seen in schwannoma, were present. The focal positivity of S-100 and CD34 in 2 cases raises the possibility of malignant peripheral nerve sheath tumor (MPNST). In these 2 cases, H3K27me2 immunostain was retained ruling out MPNST. More importantly, ultrastructural studies on all cases showed the characteristic intercellular junctions of meningiomas.

Conclusions: Meningiomas may express aberrant immunophenotype raising the possibility of alternative diagnoses. In this study, we encountered CD34 and/or S-100 positivity in 17 meningiomas necessitating additional immunostains and confirmatory EM for final diagnosis. Awareness of potential aberrant immunophenotype in meningiomas is crucial for accurate diagnosis.

1652 Glioblastomas with Polysomy of Long Arm of Chromosome 19 Often Show Ependymal and Oligodendroglial Differentiation by morphology and immunohistochemistry

Stephanie Livingston[1], Anas Bernieh[2], Siraj El Jamal[3], Ali Saad[4]
[1]University of Tennessee Health Science Center, Memphis, TN, [2]University of Mississippi Medical Center, Jackson, MS, [3]Icahn School of Medicine at Mount Sinai, New York, NY, [4]Methodist/LeBonheur Health System, Memphis, TN

Disclosures: Stephanie Livingston: None; Anas Bernieh: None; Siraj El Jamal: None; Ali Saad: None

Glioblastoma, the most common malignant primary brain tumor in the adult population, may display a wide variety of histomorphologic characteristics. The presence of certain morphologic characteristics such as small cell, rhabdoid/epithelioid, or giant cell is well documented. However, there is no correlation between these histological variants and a particular chromosomal abnormality(s). We have identified a characteristic phenotype in glioblastoma harboring polysomy of the long arm of chromosome 19 (19q) consisting of frequent display of oligodendroglial and ependymal differentiation by morphology and immunohistochemistry. The presence of ependymal differentiation, particularly in small biopsy specimens, may result in erroneous diagnosis. Glioblastoma cases with polysomy 19q are collected from various institutions. A representative block from each case is immunostained with glial fibrillary acidic protein (GFAP), epithelial membrane antigen (EMA), and Olig2. Fluorescent in situ hybridization (FISH) to test for 1p19q co-deletion (required to rule out oligodendroglioma) and loss of CDKN2A (characteristically observed in supratentorial ependymoma) was performed on all cases. The search resulted in 13 glioblastoma cases (8 males and 5 females-median age: 53.2 years). All cases were supratentorial in location. In all cases, histological examination showed tumor necrosis and/or vascular proliferation. All cases showed, at least focally, histological features suggestive of oligodendroglial differentiation i.e. tumor cells with perinuclear halo and/or delicate “chicken wire” capillaries network which triggered FISH testing for 1p19q co-deletion. In addition, 10 cases showed foci of ependymal differentiation including perivascular pseudorosettes, solid islands with a fibrillary stroma, and tumor cells oval nuclei and finely granular chromatin. By immunohistochemistry, GFAP positivity varied between the cases and also within each case. In 4 cases, GFAP was diffusely positive and in 9 cases it was focal. Olig2 showed patchy positivity in 7 cases and diffuse positivity (in nearly all tumor cells) in 6 cases. Diffuse olig2 positivity has traditionally been associated with oligodendroglioma. EMA showed microscopic foci of intracytoplasmic microrosettes in 8 cases, a feature commonly seen in ependymomas, and was negative in 5 cases. FISH studies showed all cases to be negative for 1p19q co-deletion and for CDKN2A

deletion ruling out oligodendroglioma and ependymoma, respectively. Glioblastoma with polysomy of 19q frequently display phenotypical features suggestive of oligodendroglioma or ependymoma. The former triggers FISH testing for 1p19q co-deletion. However, the latter may result in erroneous diagnosis of anaplastic ependymoma. Awareness of these phenotypical aberrations in glioblastoma is important to clinch the correct diagnosis.

1653 Histological and Molecular Evaluation of IDH-Wildtype Glioblastoma with FGFR3-TACC3 Fusion

Osorio Lopes Abath Neto[1], Liqiang Xi[2], Snehal Patel[3], Terri Armstrong[1], Mark Gilbert[1], Jing Wu[1], Kenneth Aldape[1], Mark Raffeld[4], Martha Quezado[1]
[1]National Institutes of Health, Bethesda, MD, [2]National Cancer Institute/National Institutes of Health, Bethsda, MD, [3]National Institutes of Health/National Cancer Institute, Bethesda, MD, [4]National Cancer Institute, Bethesda, MD

Disclosures: Osorio Lopes Abath Neto: None; Liqiang Xi: None; Mark Raffeld: None; Martha Quezado: None

Background: The aberrant fusion protein FGFR3-TACC3 is rarely identified in IDH-wildtype glioblastoma (GBM), with reported incidences varying between 1 and 3%. This fusion protein, which has constitutive kinase activity and induces aneuploidy, is a potential therapeutic target, as its inhibition has been shown to prolong survival in mouse models of GBM. Recent studies have suggested that tumors with *FGFR3-TACC3* fusion share common histological and immunohistochemical features. Here we present the full morphological and molecular characterization of 4 cases with the fusion protein.

Design: We established a cohort of 117 cases of IDH-wildtype GBM, determined by immunohistochemical (IHC) studies, and tested for the presence of the *FGFR3-TACC3* fusion using a customized next-generation sequencing panel, which included sequencing of genomic regions known to be associated with brain tumors. Cases had been worked up with histological processing and IHC studies for IDH1 R132H, ATRX, p53, GFAP, CD34, neurofilament protein, and MIB-1, and interpreted by an experienced neuropathologist.

Results: We identified four GBM cases (4/117, 3.4%) harboring the *FGFR3-TACC3* fusion. In all four cases, the fusion involved exon 17 of *FGFR3*, while the junction point in *TACC3* was variable. Additional findings on the molecular testing included the presence of the *TERT* promoter C228T variant in 2 cases, and significant point mutations in *CDKN2A*, *PIK3CA*, *PTEN*, and *IGF1R* in individual cases. None of the cases had *EGFR* amplification. All four cases (4/4) showed monomorphic round to ovoid, oligodendroglioma-like nuclei. Calcifications were identified in two cases (2/4), nuclear palisading in areas devoid of necrosis in three cases (3/4), and a network of branching delicate capillaries, highlighted by CD34 immunostain, in three cases (3/4). MIB-1 immunostain showed a high proliferative rate index in three cases (3/4).

Conclusions: We found *FGFR3-TACC3* fusions to be rare in our IDH-wildtype GBM cohort, similar to what has been previously reported, but our series had higher MIB-1 proliferative rates. The histological findings of our *FGFR3-TACC3* fusion cases are also in keeping with prior descriptions, supporting the use of morphological features (monomorphic round nuclei, calcifications, nuclear palisading, and delicate capillary network) to screen GBM cases to test for the fusion.

1654 Evaluation and Validation of the NGS panel CNSeq for Detecting H3 K27M Variants in Glial Tumors

Joshua Lorenz[1], Elizabeth Cochran[1], Jason Jarzembowski[1], Alexander Mackinnon[1]
[1]Medical College of Wisconsin, Milwaukee, WI

Disclosures: Joshua Lorenz: None; Elizabeth Cochran: None; Jason Jarzembowski: None; Alexander Mackinnon: None

Background: Mutations in histone variants H3.3 and H3.1 have prognostic value in pediatric glioblastomas and diffuse intrinsic pontine gliomas. These mutations are highly specific to lesions arising in the midline and associated with a rapidly fatal course. IHC has been used to identify the presence of *H3 K27M* mutations. However, the location of these lesions poses significant technical challenges in obtaining adequate tissue for diagnostic purposes. Therefore, it is useful to develop multiplex assays for mutation identification for these types of diagnostic samples characterized by limited tissue. A novel next generation sequencing (NGS) panel was developed, referred to as CNSeq, providing a viable alternative for identifying *H3 K27M* and a variety of other mutations. The goals of this project are twofold: Determine the performance of the CNSeq panel for detecting *H3 K27M* variants and validate *H3 K27M* for routine clinical use.

Design: 7 cases with H3 K27M variant (determined by testing at an outside clinical reference lab) were identified in the institutional archives. IHC was performed using an H3 K27M mutation specific antibody (rabbit polyclonal ABE419, Millipore). A targeted, AmpliSeq NGS panel (CNSeq) was designed to target hotspot or whole coding regions of 10 genes including H3. Tissue was macrodissected from tumor rich regions of unstained slides, and DNA was extracted. Libraries were constructed and templated using the IonChef. Samples were sequenced on the IonTorrent PGM. VCF files were loaded into a custom analysis pipeline and alignment pileups were manually reviewed for the *H3 K27M* variant.

Results: All 7 cases stained positive for *H3 K27M*. On average, >1000 total reads were obtained, however >90% of the reads were filtered by default TMAP filter settings. The VCF identified the variant for 2 of 7 cases, and manual inspection of the alignment pileup in IGV identified the H3 K27M variant all 7 cases. The VAF ranged from 0.25 to 0.74 with an average depth of 40 reads.

Case	K27M called by default variant caller	Mutant Visible in IGV	Total Number H3F3A Amplicons	Mutant Reads	Reference Reads	VAF
CK1	N	N	29	0	29	0
CK2	N	N	16	0	16	0
H1	Y	Y	66	20	46	0.30
H2	Y	Y	105	28	77	0.27
H5	N	Y	23	17	6	0.74
H6	N	Y	30	14	16	0.47
H7	N	Y	32	15	17	0.47
H8	N	Y	21	10	11	0.47
H9	N	Y	32	12	20	0.38

Conclusions: *H3 K27M* variant can be detected using NGS. However, most reads are filtered using default TMAP setting and are not present in the VCF. This is likely due to the high GC content and homopolymers in this region. Creating a hotspot file for this locus requires >50 reads and therefore is unlikely to increase sensitivity. Increased sensitivity can be best achieved by empirically relaxing TMAP filter settings for the targeted amplicon.

1655 An Institutional Experience with Pyrosequencing for MGMT Promoter Methylation Analysis

Ernest Nelson[1], Stephen Bagley[2], Christopher Watt[2], MacLean Nasrallah[1]
[1]University of Pennsylvania, Philadelphia, PA, [2]Hospital of the University of Pennsylvania, Philadelphia, PA

Disclosures: Ernest Nelson: None; MacLean Nasrallah: None

Background: Standard of care for treatment of glioblastoma is radiotherapy with temozolomide. Promoter hypermethylation of the *O[6]-methylguanine-DNA-methyltransferase* (*MGMT*) gene is a biomarker of tumor response to temozolomide. Although the number and combination of methylated CpG islands resulting in transcriptional silencing of *MGMT* has not been fully elucidated, several CpG sites in differentially methylated region 2 (DMR2) play a critical role in transcriptional control of *MGMT*. Most assays, including that at our institution, evaluate methylation levels in DMR2. DNA extracted from paraffin-embedded tissue undergoes bisulfite conversion, PCR amplification, and pyrosequencing to generate quantitative data for the level of methylation at four CpG sites. Given the heterogeneity in methylation at each site, mean and median levels are obtained from replicate reactions and the aggregate data is converted into a qualitative result: positive, low positive, not detected and indeterminate. While results of “positive” or “not detected” are regularly used in clinical practice to guide patient management, the implications of a result of “low positive” are unknown.

Design:

Results: We analyzed the methylation results and clinical outcomes of 195 patients with *IDH*-wildtype glioblastoma. Within our cohort, 64 patients (33%) were positive for *MGMT* promoter hypermethylation, 89 (46%) not detected, 28 (14%) low positive, and 14 (7%) indeterminate. Log-rank tests determined that median overall survival (OS) of low positives and positives was similar (29 vs. 17 months, p=0.25) and that median OS was superior in low positives compared to not detected (29 vs. 14 months, p=0.015). Using a Cox proportional hazards model to adjust for age, sex, extent of surgical resection, and performance status, both *MGMT* promoter methylation positive and low positive remained associated with improved OS compared to “not detected” (positive, HR 0.39, 95% CI 0.21-0.73; low positive, HR 0.15, 95% CI 0.05-0.48).

Conclusions: The robustness of the pyrosequencing method, resulting mean and median of methylation levels across multiple heterogeneously methylated CpG sites, appears to increase the range of clinically significant results, and may allow the development of currently lacking unified standards for assessing methylation.

1656 Utility of Glioseq Next-Generation Sequencing for Molecular Classification of Ependymomas

Marina Nikiforova[1], Abigail Wald[1], Wayne Ernst[1], Somak Roy[1], Yuri Nikiforov[1]
[1]University of Pittsburgh Medical Center, Pittsburgh, PA

Disclosures: Marina Nikiforova: None; Abigail Wald: None; Wayne Ernst: None; Somak Roy: None; Yuri Nikiforov: None

Background: Ependymomas were recently re-classified into nine molecularly distinct groups based on genomic findings, anatomical compartments, and histopathological and clinical features [PMID: 25965575]. This molecular classification started to be integrated into the World Health Organization classification of central nervous system tumors and may help with accurate diagnosis, treatment and surveillance of patients with ependymoma. In this study, we evaluated the clinical utility of GlioSeq next-generation sequencing (NGS) test for molecular classification of ependymal tumors.

Design: A total of 25 ependymoma tumor specimens, including 9 pediatric and 16 adults, were analyzed by GlioSeq® NGS test. GlioSeq is designed to interrogate CNS tumor-related alterations in small stereotactic biopsies and surgically resected tumor samples. It performs targeted sequencing of 30 genes for SNVs and indels, 24 genes for copy number alterations, and 104 genes for fusions, including *RELA* and *YAP1* fusions.

Results: Out of 25 ependymomas (EPN), 7 were from the spine (SP), 12 from the posterior fossa (PF), and 6 from the supratentorial (ST) compartment. GlioSeq genomic profiling allowed to classify into molecular groups 19 out of 25 (76%) of ependymomas. Based on the presence of NF2 mutations and copy number alterations, 5 (71%) of the spinal ependymomas were classified into 4 SP-EPN (anaplastic ependymoma, NF2 positive) and one SP-MPE (myxopapillary ependymoma with chromosomal instability). The posterior fossa ependymomas demonstrated a stable genome in 6 adult patients that led to classification into 6 PF-EPN-A (anaplastic ependymoma with balanced genome) and showed an unstable genome in 2 patients (PF-EPN-B, anaplastic ependymoma with chromosomal instability). Finally, 6 (100%) supratentorial ependymomas were positive for C11orf95/RELA fusion, allowing classification into ST-EPN-RELA (anaplastic ependymoma *RELA* fusion positive) subgroup.

Conclusions: GlioSeq NGS test was able to establish molecular classification in the majority (76%) of resection and biopsy samples of ependymoma, which helps personalize clinical management of pediatric and adult patients with this tumor.

1657 Energy Metabolism Deficits in Alzheimer Disease

Vihar Patel[1], Thomas Raife[2], Shahriar Salamat[2], Ozioma Okonkwo[2], Jonathan Stefely[3]
[1]Madison, WI, [2]University of Wisconsin, Madison, Madison, WI, [3]University of Wisconsin, Madison, New Glarus, WI

Disclosures: Vihar Patel: None; Ozioma Okonkwo: None; Jonathan Stefely: None

Background: The understanding of Alzheimer disease (AD) has been dominated by the amyloid hypothesis. However, clinical trials targeting beta-amyloid have largely failed, sparking interest in other potential factors such as the link between energy metabolism abnormalities and AD. The biological variability and heritability of erythrocyte energy metabolism suggests the possibility of a similar variability in AD. The current study explored the biological variability of brain and erythrocyte energy metabolism in AD and non-AD control subjects (CTRL), under the premise that the heritable energy metabolism pathways in erythrocytes reflects energy metabolism in brain.

Design: Untargeted metabolomic scans of prefrontal cortex and blood were performed using autopsy specimens of 10 subjects with histologically documented AD (NIA-AA Score of A3B3C3) and 10 age and gender-matched CTRL subjects without AD. Metabolite profiles in energy metabolism pathways were analyzed in brain and blood of AD vs. CTRL groups with a focus on comparative differences in glucose and ketone metabolism. Statistical analyses were performed using XLSTAT.

Results: Of the 445 named biochemicals detected in both tissues, 131 were significantly correlated between brain and blood ($p<0.05$). Comparison of metabolites in AD and CTRL groups revealed a broad reduction in the relative abundance of energy-related biochemicals in AD brain. Figure 1 shows the biological variation and statistical significance of metabolites in the blood and brain of AD vs. CTRL. Figure 2 shows decreased glycolytic intermediates in the brain of AD vs. CTLR with a mean 1.9-fold difference ($p<0.017$). The ketone body beta-hydroxybutyric acid (BHBA) was highly correlated between brain and blood samples ($R^2 = 0.98$); the median relative abundance was 3.5-fold higher in CTRL brain and 7.6-fold higher in CTRL blood ($p<0.01$).

Figure 1 - 1657

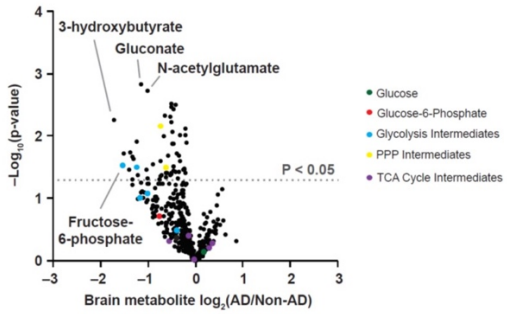

Figure 1. A volcano plot showing the fold-change and statistical significance of metabolites in the blood and brain of AD vs. Non-AD (CTRL). Metabolites above the gray dotted line are statistically significant ($p<0.05$). On the X-axis, metabolites with negative values are decreased in AD vs. Non-AD. Metabolites are color-coded based on pathways involved.

Figure 2 - 1657

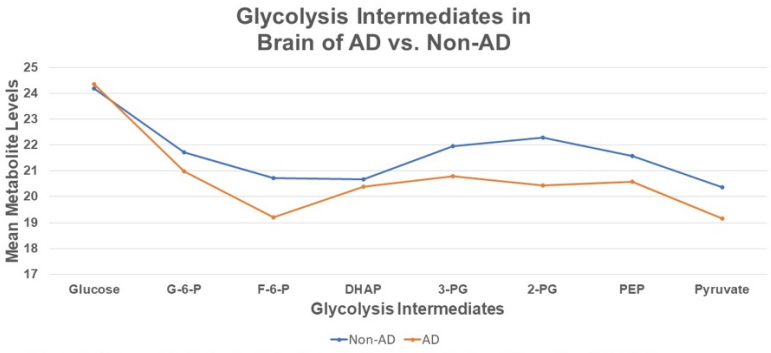

Figure 2. Mean metabolite levels of glycolysis are decreased in brains of AD vs. Non-AD (CTRL). Mean metabolite levels are Log2 transformed. G-6-P = Glucose-6-Phosphate, F-6-P = Fructose-6-Phosphate, DHAP = Dihydroxyacetone phosphate, 3-PG = 3-phosphoglycerate, 2-PG = 2-phosphoglycerate, PEP = Phosphoenolpyruvate

Conclusions: Metabolites in glucose energy metabolism pathways are consistently decreased in the brain of AD compared to non-AD subjects. Together with significantly decreased levels of BHBA in brain and blood of AD, our findings strongly suggest an important contribution of systemic impairments in energy metabolism in AD pathology.

1658 Prevalence of Mismatch Repair Gene Mutations in Uveal Melanomas: A Retrospective Analysis of 1230 Cases

Samantha Phou[1], Kyle Fraser[2], John Thorson[2], Jonathan Lin[3]
[1]University of California, San Diego, San Diego, CA, [2]University of California, San Diego, La Jolla, CA, [3]La Jolla, CA

Disclosures: Samantha Phou: None; Kyle Fraser: None; John Thorson: None; Jonathan Lin: None

Background: Germline mutations in mismatch repair genes and microsatellite instability have been implicated in the development of numerous malignant neoplasms such as colon and ovarian cancers. Low frequency microsatellite instability has been reported as an infrequent event in uveal melanomas, yet the frequency of mismatch repair defects in uveal melanomas has yet to be determined. In this study, we reviewed 1230 uveal melanoma cases to identify mutations in mismatch repair genes.

Design: We examined uveal melanoma cases identified at the University of California, San Diego (UCSD) and from online cancer sequencing database portals. We queried for mutations in six well-defined mismatch repair genes: *PMS1*, *PMS2*, *MSH2*, *MSH3*, *MSH6*, and *MLH1*. Data was obtained from next generation sequencing of a panel of cancer-related genes as well as cytogenetic microarray analysis of 9 cases identified at UCSD from 2016-2018. In addition, sequencing and cytogenetic data from 80 specimens were obtained from The Cancer Genome Atlas (TCGA) and from 1141 specimens from the Catalogue of Somatic Mutations in Cancer (COSMIC).

Results: We identified one *PMS1* mutation resulting in a truncating mutation (1/9 UCSD cases; 0/159 COSMIC cases; and 0/80 TCGA cases, all tested for *PMS1* mutations). We identified one in-frame deletion in *MSH3* (0/9 UCSD; 1/115 COSMIC; 0/80 TCGA). No mutations were identified in *PMS2* (0/9 UCSD; 0/159 COSMIC; 0/80 TCGA). No mutations were identified in *MSH2*, *MSH6*, or *MLH1* (0/9 UCSD; 0/250 COSMIC; 0/80 TCGA). Monosomy 3, including the loss of *MLH1*, was identified in 3/9 UCSD cases (33%), 39/78 TCGA cases (50%), and 144/179 COSMIC cases (80%) with reported cytogenetic data. Partial monosomy 3, with unclear status of the loss of *MLH1*, was reported in 7/179 COSMIC cases. One TCGA case with the loss of 3q but unknown status of 3p was identified.

Conclusions: We conclude that somatic or germline mutations in mismatch repair genes are very rare events in uveal melanomas. A surprising exception is the *MLH1* mismatch repair gene, where loss of one copy of *MLH1* (3p.22.2) arises through monosomy 3, a common cytogenetic mutation in uveal melanomas. Monosomy 3 also results in the loss of the *BAP1* tumor suppressor gene (3p21.1). The concomitant loss of *MLH1* and *BAP1* with monosomy 3 raises the possibility that the loss of *MLH1* may synergize with the loss of *BAP1*, contributing to the known aggressive nature of uveal melanomas with monosomy 3.

1659 Clinical and Pathological Features of 19 Eyelid Pilomatrixomas

Sepideh Siadati[1], Charles Eberhart[1]
[1]Johns Hopkins University School of Medicine, Baltimore, MD

Disclosures: Sepideh Siadati: None; Charles Eberhart: None

Background: Pilomatrixoma is a relatively rare skin tumor arising from matrix of hair root. It is found most commonly on the head and neck as well as upper extremities. In the periocular region, most involve eyebrow, and the eyelid is a less common site. Only a few case series of eyelid pilomatrixoma have been published. Here we present clinical and histological data from 19 eyelid pilomatrixoma.

Design: Eyelid pilomatrixoma cases diagnosed at our institution since 1981 were identified via electronic medical records. All slides were reviewed, and demographic as well as clinical data obtained.

Results: Patient ages ranged from 2 to 63 years (mean 24 years, median 14 years), including 12(63%) females and 7(37%) males. Eight (42%), and 4(21%) cases arose in the first and second decades of life, respectively. Twelve tumors were found in the left eye and 7 in the right, with 14 and 5 in the upper and lower lids, respectively. All eyelid pilomatrixoma presented as solitary lesions, although one patient had a second pilomatrixoma in the left temple. One case involved the lash line at the lid margin. Initial clinical diagnoses included chalazion suspicious for sebaceous carcinoma (1 case), sebaceous cyst (2 cases), dermoid cyst (1 case), cystic lesion (4 cases), and suspicious nodule (11 cases). Skin overlying two cases showed hypervascularity and dilated vessels. The lesions varied from 2 mm to 12 mm in maximum dimension. Microscopically, the tumors were relatively typical pilomatrixoma with basaloid and shadow cells accompanied by calcification and foreign body giant cells. However, mixed acute and chronic inflammation was noted in 1 case, acute inflammation in 3, hemosiderin laden macrophages in 1, and in 4 cases (21%) basaloid cells were absent. All tumors were located in the lower dermis or subcutaneous tissues, except for 1 case centered in the upper dermis.

Conclusions: Eyelid pilomatrixoma is a rare eyelid tumor, with approximately 60% of cases presenting in the first two decades of life and a slight female predominance. Eyelid pilomatrixoma are rarely suspected clinically, and can be mistaken for cyst, chalazion, sebaceous carcinoma and other tumors. Physicians should be aware of the possibility of pilomatrixoma in eyelid area, especially in a child or young patient. Complete excision is curative and diagnosis can generally be established by histopathological examination.

1660 The Role of pY705-Stat3 Immunohistochemistry in Glioblastoma Prognosis

Sergiu Susman[1], Adriana Olar[2], Radu Pirlog[1], Andrei Mitre[3], Stefan Ioan Florian[3]
[1]University of Medicine and Pharmacy "Iuliu Hatieganu", Cluj Napoca, Romania, [2]Medical University of South Carolina, Charleston, SC, [3]University of Medicine and Pharmacy "Iuliu Hatieganu", Cluj-Napoca, Romania

Disclosures: Sergiu Susman: None; Adriana Olar: None; Radu Pirlog: None; Andrei Mitre: None; Stefan Ioan Florian: None

Background: Glioblastoma is classified as a grade IV glioma by the current WHO 2016 classification of brain tumors and is known to be the most lethal cancer in the brain. It is characterized by a distinct histological appearance including the presence of necrosis and microvascular proliferation, which reflects an intra-tumoral heterogeneity regarding the cellular adaptation to hypoxia. Recent studies that tried to decode the molecular mechanisms involved in the cellular adaptation to hypoxia in glioblastoma evidenced that the principal pathways activated under hypoxia are hypoxic inducible factor 1α (HIF-1α), vascular endothelial growth factor (VEGF), transforming growth factor beta (TGFb), but also signal transducer and activator of transcription 3 (Stat3).

Design: Ninety-one glioblastoma samples were included in this retrospective study. Paraffin-embedded tissue samples from the archives of the Department of Pathology were obtained from patients undergoing surgery for glioblastoma between 2009 and 2015 in the Department of Neurosurgery, Emergency County Hospital, Cluj-Napoca. The immunohistochemistry staining was performed automatically with DAKO Omnis®, using EDTA, pH 9, for antigen retrieval, at dilution of 1:400. We assessed the percentage of Stat3 positive tumor cells (0–100%) and intensity of the immunostaining. The H-score was calculated for all subjects. We considered a 20% positivity of tumor cells as a cutoff for STAT3 immunopositivity. Patients' OS was analyzed using Kaplan-Meier method and long-rank tests. All analyses were performed in R environment.

Results: Statistical analysis allowed us to define 2 groups, considering a cut-off of 20% pY705-Stat3 positive cells. We found a statistical significant survival difference between Group 1 (with less than 20% of positive cells) with 13.7 months and 8.9 months for Group 2 (with more than 20% of positive cells), $p<0.001$, log-rank test.

On multivariate analyses with the COX proportional hazards regression model including Stat3 expression, age and relapse, Stat3 expression was an independent prognostic factor in glioblastoma ($P<0.001$).

Conclusions: Our results show that pStat3Tyr705 can be easily evaluated by IHC and has an important prognostic role in GBM. Stat3 positive expression is associated with significant shorter overall survival independent of age and relapse status.

1661 Immunohistochmenical Analysis of Endothelial GLUT1 Expression in Cerebral Vascular Malformations

Toyohiro Tada[1], Satoshi Baba[2], Hisashi Tateyama[3], Takashi Tsuchida[2], Megumi Yoshida[3], Misawo Ishikawa[4], Takashi Matsumoto[5]

[1]Toyokawa City Hospital, Toyokawa-shi, Japan, [2]Hamamatsu University Hospital, Hamamatsu, Japan, [3]Kasugai City Hospital, Kasugai, Japan, [4]Nagoya City, Japan, [5]Toyokawa City Hospital, Toyokawa, Japan

Disclosures: Toyohiro Tada: None; Satoshi Baba: None; Hisashi Tateyama: None; Takashi Tsuchida: None; Megumi Yoshida: None; Misawo Ishikawa: None

Background: Cerebral vascular malformations (CVMs) are classified into arteriovenous (AVMs) or cavernous malformations (CMs). Only two immunohistochemical studies on endothelial glucose transporter protein 1 (GLUT1) expression in CVMs exist: one found no expression in CMs (n=20), while the other demonstrated endothelial cell (EC) immunostaining in both AVMs (n=3) and CMs (n=3). GLUT1 is expressed in mature endothelial cells of blood vessels in the central nervous system (CNS). In contrast, ECs of other organs/tissues, except infantile hemangiomas (IHs) and verrucous hemangiomas, do not express GLUT1. The aim of this study was to investigate the immunohistochemical expression of GLUT1 in CVM endothelium in a large case series.

Design: Surgical specimens of 36 cases of brain CVMs, composed of AVM (n=23) and CM (n=13), were diagnosed histologically using elastic and H&E stains, and a smooth-muscle cell (h-caldesmon) immunostain. All specimens were stained immunohistochemically with antibodies to GLUT1 and EC markers (CD31, CD34, and podoplanin). Controls were: extracerebral vascular malformations (n=25) including intramuscular and cutaneous cases, and IHs (n=3). Immunopositive endothelium was quantitated as a percentage by measuring the length of positive endothelium of malformed vessels relative to the whole length of malformed vessels. Scores were: 0, <5%; 1+, 5–30%; 2+, 31–70%; 3+, 71 to 100% (Table 1).

Results: All cases of CVMs showed the immunohistochemical expression of endothelial GLUT1 in AVMs and CMs. Notably, GLUT1 in CMs showed much higher positivity (3+) than that of AVMs (Table 1). In AVMs, the endothelium of venous vessels was more frequently positive for GLUT1 than that of arterial vessels. CD31 was constantly well stained, mainly with a high score (3+). Unexpectedly, CD34 was almost negative (score 0) in two cases of AVM (9%). Unlike CD31, the extent of CD34 and GLUT1 expression was diverse in every case. Eleven AVM cases (48%) showed complementary GLUT1 and CD34 expression in the some foci, unlike in CMs. Podoplanin (D2-40) was negative (0%) in all cases of CVM. All controls except IHs were completely negative for GLUT1.

Table 1

	AVM (n=23)			CM (n=13)		
	IHC positivity# (percentage)			IHC positivity# (percentage)		
Antibody	1+ *	2+**	3+***	1+*	2+**	3+***
GLUT1	n=5 (22%)	n=11 (48%)	n=7 (30%)	n=2 (15%)	n=2 (15%)	n=9 (70%)
CD34	n=2 (9%)	n=11 (47%)	n=8 (35%)	n=0 (0%)	n=1 (8%)	n=12 (92%)
CD31	n=0 (0%)	n=3 (13%)	n=20 (87%)	n=0 (0%)	n=0 (0%)	n=13 (100%)
Complementary expression of GLUT1 and CD34	n=11 (48%)			n=0 (0%)		

Ratio (percentage) of the length of positive endothelium to the whole length of endothelium in malformed blood vessels.

*1+: 5 to 30%, **2+:31 to 70%, ***3+: 71 to 100%

AVM, cerebral arteriovenous malformation; CM, cerebral cavernous malformation; GLUT1, glucose transporter protein 1; IHC, immunohistochemistry

Conclusions: GLUT1 is a unique endothelial marker for CVMs of the CNS that is never expressed in other extracerebral vascular malformations. Etiologically, endothelial GLUT1 expression in CVMs suggests that malformed vessels may be associated with original (normal) brain blood vessels. The significance of complementary expression of GLUT1 and CD34 remains obscure.

1662 Neuropathology Findings in Patients with History of Ventricular Assist Devices

Matthew Torre[1], Jeffrey Helgager[1], David Meredith[2], Robert Padera[3]
[1]Brigham and Women's Hospital, Harvard Medical School, Brookline, MA, [2]Boston, MA, [3]Brigham and Women's Hospital, Boston, MA

Disclosures: Matthew Torre: None; Jeffrey Helgager: None; David Meredith: None; Robert Padera: None

Background: Ventricular assist devices (VADs) provide circulatory support for patients with advanced heart failure and are often used as a bridge to heart transplant. VADs have been associated with multiple adverse neurological outcomes, including stroke, hemorrhage, and neurocognitive deficits. In this series of postmortem cases, we describe the neuropathologic findings in VAD patients and provide clinicopathologic correlations between these findings and the VAD design and the duration of VAD use.

Design: Autopsy CNS tissue for all patients with a history of VADs collected within a 27-year period at a single tertiary care institution was reviewed for gross and microscopic evidence of hypoxic-ischemic and hemorrhagic lesions. The prevalence of these findings was compared to a control autopsy group of patients with history of cardiomyopathy/atherosclerosis and a second control autopsy group of patients with no significant cardiac history.

Results: 38 patients with a history of VADs were identified (22 with pulsatile VADs, 14 with continuous flow VADs, and 2 with history of both). Duration of VAD use ranged from 3 days to 6 years. VAD patients had a higher prevalence of macroinfarcts (63.2%) compared to control cardiomyopathy/atherosclerosis patients (33.3%) and control patients with no significant cardiac history (20.7%). VAD patients also had a higher rate of microinfarcts compared to control patients with no significant cardiac history (39.4% versus 10.3%) but had a similar rate compared to the control cardiomyopathy/atherosclerosis patients (33.3%). The presence of thrombus within the VAD at time of explant or autopsy, seen in 13 cases, was correlated with higher incidence of macroinfarcts (84.6% versus 54.5%) but not microinfarcts (38.5% versus 36.4%). Compared to pulsatile VADs, continuous flow VADs were associated with higher incidence of microinfarcts (57.1% versus 27.2%), similar rates of macroinfarcts (57.1% versus 63.3%), and lower rates of hemorrhage (14.3% versus 27.2%). Longer duration of VAD use was associated with increased prevalence of macroinfarcts, but there was no clear trend for microinfarcts. Age, sex distribution, and number of examined slides were comparable among all groups.

Conclusions: VADs are integral for the management of refractory heart failure. The use of VADs is associated with an increased incidence of a range of hypoxic-ischemic insults to the CNS. Differences in VAD design may predispose patients to different patterns of CNS pathology.

1663 Clinicopathologic Features and Assessment of ADAM3A Gene Copy Gain by FISH in Conjunctival Squamous Cell Carcinoma and its Precursor Lesions (Carcinoma in Situ/Conjunctival Intraepithelial Neoplasia)

Maria Adelita Vizcaino Villalobos[1], Abeer Tabbarah[2], Laura Asnaghi[1], Antje Arnold[3], Charles Eberhart[1], Fausto Rodriguez[4]
[1]Johns Hopkins University School of Medicine, Baltimore, MD, [2]American University of Beirut, Beirut, Lebanon, [3]Baltimore, MD, [4]Johns Hopkins University, Baltimore, MD

Disclosures: Maria Adelita Vizcaino Villalobos: None; Abeer Tabbarah: None; Laura Asnaghi: None; Antje Arnold: None; Charles Eberhart: None; Fausto Rodriguez: None

Background: Conjunctival squamous cell carcinoma (cSCC) and its precursors are among the most frequent ocular surface neoplasms worldwide, but little is known about their molecular drivers. *ADAM3A* gene (A Disintegrin And Metalloprotease Domain 3a) is part of a family that encodes a protein with both potential adhesion and protease domains and was initially described in spermatogenic cells. Amplification of this gene has been reported in neoplasms like nasal NK/T cell lymphoma. Additionally, copy gain of 8p11.22 and *ADAM3A* overexpression has been also recently identified in invasive cSCC. The aims of this study were to confirm *ADAM3A* alterations in conjunctival intraepithelial neoplasia (CIN), carcinoma in situ (CIS), and invasive cSCC, and to assess these alterations in earlier stages of conjunctival squamous neoplasia and non-neoplastic conjunctiva, as well as their potential as a diagnostic biomarker.

Design: A cohort of 55 cases from a ten-year retrospective review of the clinical and pathology records and histologic confirmation was analyzed. Using fluorescent in situ hybridization (FISH), we evaluated *ADAM3A* status in 30 cases using an 8p11 locus probe and a chromosome 8 (Chr 8) centromere reference probe. Adjacent, non-neoplastic conjunctiva and three pterygia were also tested as controls. Gains were defined with a target/control probe ratio >1.2, while high-level amplification was defined as a ratio >2.

Results: Eighty two percent (45/55) of the cases of cSCC and its precursors presented in men and 18% (10/55) in women. The age at presentation ranged from 12 to 94 years (mean 64.9 years). Severe CIN was diagnosed in 46% (25/55) of the cases, followed by CIS in 31% (17/55), moderate CIN in 15% (8/55), invasive cSCC in 7% (4/55), and mild CIN in 1% (1/55). Nine out of 30 (33%) cases showed *ADAM3A* alterations. Seven out of 9 (78%) altered cases harbored either *ADAM3A* or Chr 8 gains, while monosomy 8 was

detected in 2 out of 9 (22%) cases. Both gains and monosomy were more frequent in severe CIN (6/9, 70%). No *ADAM3A* alterations were detected in non-neoplastic controls.

Figure 1 - 1663

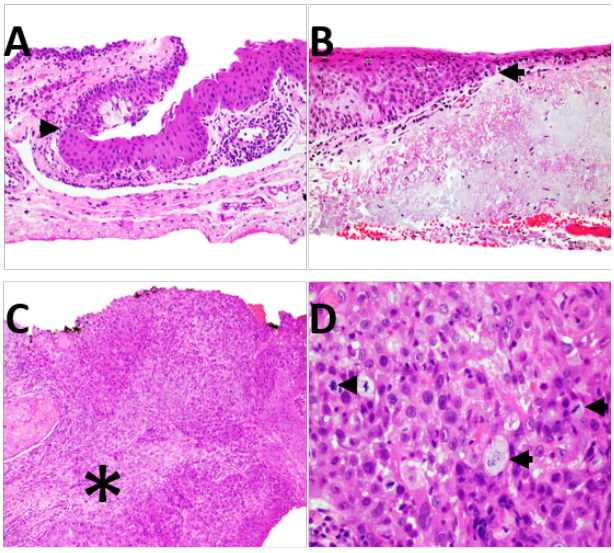

Figure 2 - 1663

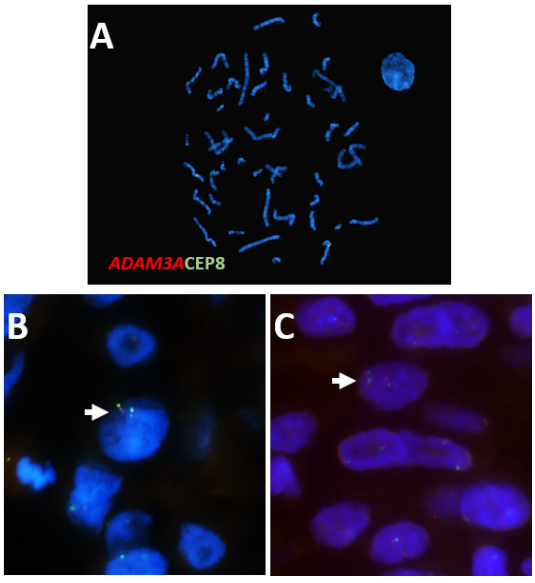

Conclusions: Gains of *ADAM3A*/chromosome 8 may be detected by FISH in a subset of cSCC and its precursor lesions (~23%). Even though high-level amplification was not identified in any case, gains were more frequent in severe CIN. *ADAM3A* alterations were limited to the neoplastic regions, sparing non-neoplastic conjunctiva and absent in tested controls. Thus, the specificity of this alteration for ocular SCC deserves further studies.

1664 The Utility of SOX2 Immunohistochemistry in Differentiating Gliosarcoma from Histologic Mimics

Jared Woods[1], Jason Hornick[2], David Meredith[3]
[1]Brigham and Women's Hospital, Boston, MA, [2]Brigham and Women's Hospital, Harvard Medical School, Boston, MA, [3]Boston, MA

Disclosures: Jared Woods: None; Jason Hornick: None; David Meredith: None

Background: Gliosarcoma is a rare variant of glioblastoma that contains areas of both glial and mesenchymal differentiation, the latter being characterized by absence of staining for glial markers such as GFAP and OLIG2. SOX2 is a transcription factor that plays a key role in pluripotency and self-renewal and has been shown to be upregulated in several aggressive primary CNS malignancies. In this study, we examine the utility of SOX2 immunohistochemistry (IHC) to identify gliosarcomas, as well as its specificity in discriminating several potential histologic mimics.

Design: IHC was performed using a rabbit polyclonal anti-SOX2 antibody (Novus Biologicals) following pressure cooker antigen retrieval (citrate buffer; pH 6.1) on 5 µm formalin-fixed, paraffin-embedded sections of gliosarcoma (n=11), melanoma (n=10), solitary fibrous tumor (n=10), malignant peripheral nerve sheath tumor (n=10), meningioma (n=10), synovial sarcoma (n=10), cellular schwannoma (n=10), and leiomyosarcoma (n=10). Nuclear staining was recorded according to extent (0, no staining; 1+/focal, <5%; 2+/multifocal, 5% to 50%; 3+/diffuse, >50%) and intensity (weak, moderate, strong); 5% or more immunoreactivity was considered positive.

Results: SOX2 staining was observed in 10 of 11 gliosarcomas. Both glial and mesenchymal components were positive; however, the mesenchymal component overall showed decreased expression. Several other tumor types also frequently exhibited diffuse staining, including cellular schwannoma (10/10), synovial sarcoma (9/10), malignant peripheral nerve sheath tumor (7/10) and melanoma (7/10). Solitary fibrous tumor (0/10), leiomyosarcoma (1/10), and meningioma (1/10) overall showed minimal SOX2 staining.

Conclusions: SOX2 is a sensitive marker for tumors of neuroectodermal derivation and is a useful ancillary marker for gliosarcomas, especially in limited biopsies or in instances of predominantly mesenchymal morphology. This study also expands the differential of SOX2-positive spindle cell neoplasms that may be encountered in the CNS to include benign and malignant nerve sheath tumors, synovial sarcoma, and melanoma.

1665 Periocular sebaceous carcinoma: analysis of intraepithelial spread and ZEB1 expression

Xinhai Zhang[1], Charles Eberhart[2]
[1]David Geffen School of Medicine at UCLA, Los Angeles, CA, [2]Johns Hopkins University School of Medicine, Baltimore, MD

Disclosures: Xinhai Zhang: None; Charles Eberhart: None

Background: Ocular sebaceous gland carcinoma (SGC) is a relatively rare tumor with worse prognosis than more common eyelid malignancies such as basal cell carcinoma. This aggressive behavior is due in part to the propensity of SGC to spread diffusely through the periocular epithelium, making it difficult to completely excise. Systemic metastasis occurs in 8-14% of cases, and 10-30% result in death. The pathological and molecular features driving intraepithelial spread are poorly understood. We present a series of cases and evaluate pathological and clinical features as well as expression of the epithelial-mesenchymal transition (EMT) factor ZEB1.

Design: We searched the electronic medical record for SGC cases diagnosed in our institution since 1991. Hematoxylin and eosin stained slides of each cases were evaluated for extent of intraepithelial spread, and immunohistochemal analysis of ZEB1 was performed in a subset.

Results: A total of 111 periocular SGC specimens from 43 patients were identified, and 35 patients had sufficient slides and other materials available for detailed analysis. These included 22 females and 13 males. The median age was 77 years (range 27 years to 98 years). 13 patients (37.1%) had the tumor centered in the lower eyelid, and 20 patients (67.2%) had the lesion centered in the upper eyelid, whereas two patients had extensive carcinoma in both upper and lower eyelids. Among the male patients, 10 (83.3%) had their lesion in the upper lids. Histologically, all of the SGC cases were poorly differentiated. They were subdivided into three groups with respect to spread: (1) purely subepithelial nodules (5 cases, 14.3%); (2) combined intraepithalial spread and subepithelial nodules (22 cases, 62.8%); and (3) exclusive intraepithelial spread (8 cases, 22.9). There was no age or gender preference in these three groups, although group 2 was more commonly seen in the upper eyelid. ZEB1 nuclear expression was noted in the subepithelial component in 1 of 14 cases evaluated, and in the intraepithelial component in 4 of 14 cases.

Figure 1 - 1665

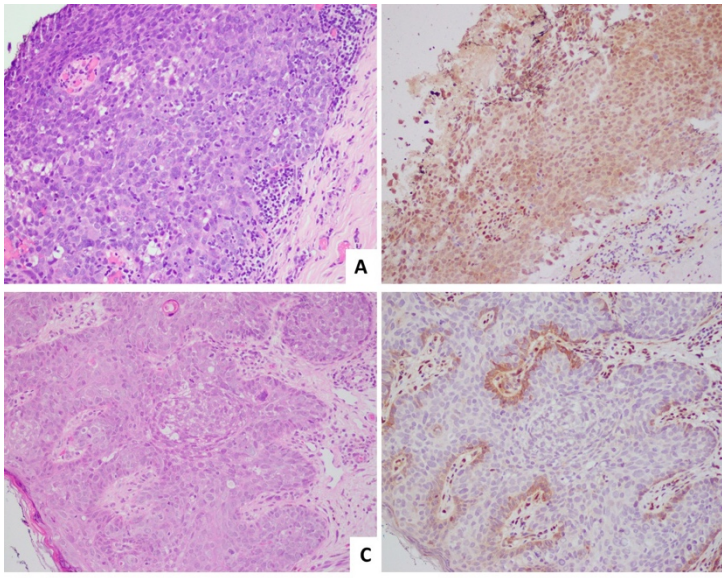

Figure 2 - 1665

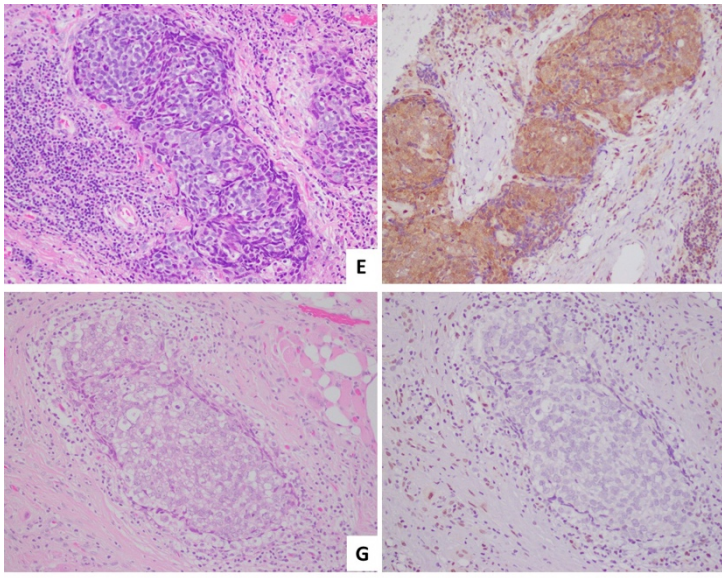

Conclusions: Ocular SBC is a rare eyelid malignancy with a median age at diagnosis of 77 years and female predominance. In our series, males were more likely to have tumor in the upper eyelids. The majority of tumors show nodular subepithelial distribution with intraepithelial spread, with purely intraepithelial carcinoma representing the second most common distribution. ZEB1 is expressed in a small subset of ocular SBC, and may play a role in tumor spread.

1666 Screening Method to Detect 1p/19q Co-Deletions by Targeted Next Generation Sequencing

Sina Zomorrodian[1], Pramod Mayigowda[2], Lan Hu[2], Alexa Buckley[3], Olena Marchenko[2], Nevenka Dimitrova[4], John T. Fallon[5], Fei Ye[6], Minghao Zhong[6]
[1]Westchester Medical Center at New York Medical College, Valhalla, NY, [2]Philips Healthcare, Valhalla, NY, [3]University of California, Berkeley, Berkeley, CA, [4]Pelham, NY, [5]New York Medical College and Westchester Medical Center, New York, NY,[6]Westchester Medical Center, Valhalla, NY

Disclosures: Sina Zomorrodian: None; Pramod Mayigowda: None; Lan Hu: None; Alexa Buckley: None; Olena Marchenko: None Nevenka Dimitrova: *Employee*, Philips Medical Systems; John T. Fallon: None; Fei Ye: None; Minghao Zhong: None

Background: The current World Health Organization (WHO) classification of central nervous system (CNS) tumors integrates morphology and molecular genetics in the diagnosis of tumors. Molecular profiling is a significant step in the diagnosis, prognosis and treatment of CNS tumors. Different genetic alterations require different methods for their detection. For example, *IDH* mutations and 1p/19q co-deletion are required tests in glioma work up. *IDH* mutations are typically point mutations and require sequencing methods such as next generation sequencing (NGS). 1p/19q co-deletions comprise large structural changes and are usually detected by a FISH assay. With advances in bio-informatics and methodology in NGS, NGS has been used to detect a diverse array of genetic alterations. Here, we test whether NGS can be used to detect 1p/19q co-deletions.

Design: The targeted NGS panel, AmpliSeq™ for Illumina Focus Panel was used. The Focus Panel is designed to sequence 52 genes and more than 200 amplicons, which covers most chromosomes. There are 3 genes and 13 amplicons located in the chromosome 1p region. The study samples include 16 normal human DNA from blood cells, 10 FFPE samples of CNS tumors with 1p/19q deletion confirmed by FISH and 140 FFPE samples of non-CNS tumors. Copy number variation (CNV) of the three genes located at chromosome 1p was first normalized (normalization for library size, GC content and amplicon length) by read coverage with 16 normal blood samples. They were subsequently assigned statistical significance resulting from the segmentation of normalized profiles and gene-aware correction of the predicted CNV.

Results: No chromosomal change was detected in the 16 normal samples (Fig. 1A). For the 140 non-CNS tumors, some chromosomal change/gene copy number variations were detected, such as Her-2 amplification (Fig. 1B) in breast cancer. For the CNS tumors, 1p deletion (Fig. 1C) was detected in all 10 cases.

Figure 1 - 1666

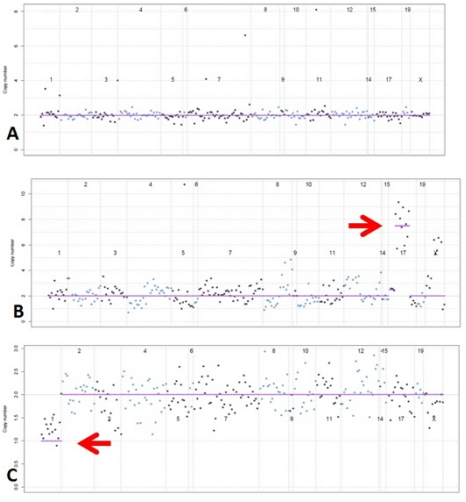

Figure 1. Each amplicon's coverage change generated by Focus panel. The x axis represents coverage/relative copy number. Y axis represents each amplicon in order from chromosome 1 to X. (A) Sample with no chromosomal change/gene copy number variations. (B) Breast cancer sample with Her-2 amplification (indicated by red arrow). (C) Oligodendroglioma sample with 1p deletion (indicated by a red arrow).

Conclusions: The Focus panel is routinely used to detect solid tumor mutations, such as IDH. We demonstrated the ability of this test to detect chromosomal change/gene copy number variations, including 1p deletion and Her-2 amplification. Therefore, the Focus panel can also function as a screening test for 1p/19q co-deletions, along with its primary function of targeted NGS sequencing, without additional costs.